Award Number 02HQGR0018

SOURCE CHARACTERISTICS OF MODERN AND HISTORICAL IN-SLAB EARTHQUAKES APPLICABLE TO STRONG-GROUND MOTION PREDICTION

Gene A. Ichinose, Hong Kie Thio, and Paul G. Somerville
URS Group, Inc.
566 El Dorado St. 2nd Floor
Pasadena, CA 91101-2560
626.449.7650 (phone)
626.449.3536 (fax)
gene_ichinose@urscorp.com (email)

Element I

Research supported by the U.S. Geological Survey (USGS), Department of the Interior, under USGS award number (Ichinose, 02HQGR0018). The views and conclusions contained in this document are those of the authors and should not be interpreted as necessarily representing the official policies, either expressed or implied, of the U.S. Government.

Award Number 02HQGR0018

SOURCE CHARACTERISTICS OF MODERN AND HISTORICAL IN-SLAB EARTHQUAKES APPLICABLE TO STRONG-GROUND MOTION PREDICTION

Gene A. Ichinose, Hong Kie Thio, and Paul G. Somerville
URS Group, Inc.
566 El Dorado St. 2nd Floor
Pasadena, CA 91101-2560
626.449.7650 (phone), 626.449.3536 (fax)
gene_ichinose@urscorp.com, hong_kie_thio@urscorp.com, paul_somerville@urscorp.com

TECHNICAL ABSTRACT

The last 3 Puget Sound in-slab earthquakes (1949 M=7.1, 1965 M_w=6.7, and 2001 M_w=6.8) produced moderate levels of ground motions below 0.3 g yet caused widespread damage and disruption to buildings and transportation lifelines. The frequency of in-slab earthquakes makes it important to understand as much as possible about the source characteristics of in-slab earthquakes so that the hazard they pose can be more reliably quantified. We first estimate the point source parameters of the 1999, 2001 Satsop, 2001 Nisqually, and 2003 Mount Olympus, Washington earthquakes. The estimates include focal-mechanism, the regional-wave moment tensor, centroid depth, and scalar seismic moment. We use the 2001 Satsop earthquake to calibrate the 1-D velocity model structure for the calculation of Green's functions using a waveform inversion method. This new model improves the fitting of amplitudes and arrival-times of major phases between synthetics and observed seismograms at frequencies of around 1 Hz. The estimated point source parameters are used in assuming the finite-fault orientation and location. We invert teleseismic P-, and SH-waves, local strong ground motion, and co-seismic horizontal displacements recorded from GPS, to estimate the slip model of the 2001 Nisqually earthquake. The local Green's functions are computed using the calibrated velocity model. We also estimate the slip model of the 1965 Seattle-Tacoma earthquake using teleseismic data from WWSSN stations.

Our goal is to accurately estimate the ground motions expected from a repeat of the 1965 Seattle-Tacoma earthquake near urban Seattle. The 1999 Satsop earthquake could be considered a repeat of the 1946 Satsop earthquake and the 2001 Nisqually earthquake could be considered a repeat of the 1949 Olympia earthquake. The Seattle-Tacoma area may therefore be likely to experience the next in-slab event within the next 30 to 50 years. We accomplish this goal by applying a modified time-domain based modeling method that uses a finite-fault rupture model, geology as a proxy for site amplification, and amplification from basin depth to estimate the ground motion levels. With these components we test the predicted ground motions with those observed in the Nisqually earthquake using a shake-map presentation. The shake-maps display the peak horizontal ground accelerations (PGA), and absolute acceleration (S_a) at periods of 0.3, 1.0, and 3 seconds for a single degree of freedom oscillator with 5% damping. Analyses of predicted and observed ground motions, for the Nisqually earthquake, suggest that the site and basin-depth amplification corrections removed the bias but not the spread of the residuals. We also found that predicted PGA correlated poorly observations but spectral acceleration performed better. We then apply the modeling method to estimate the ground motions experienced from the 1965 Seattle-Tacoma earthquake. The pattern of ground motions are very different than those predicted for the Nisqually earthquake. We can also expect ground motions in urban Seattle up to 0.6 g, twice as high as those generated by the Nisqually earthquake. The reexamination of this historical earthquake adds more realism than a scenario earthquake simulation. Shake-maps offer better portability to applications that use Geographic Information System technology such as HAZUS, developed by the Federal Emergency Management Agency to estimate the detailed losses sustained from earthquakes.

Award Number 02HQGR0018

SOURCE CHARACTERISTICS OF MODERN AND HISTORICAL IN-SLAB EARTHQUAKES APPLICABLE TO STRONG-GROUND MOTION PREDICTION

Gene A. Ichinose, Hong Kie Thio, and Paul G. Somerville
URS Group, Inc.
566 El Dorado St. 2nd Floor
Pasadena, CA 91101-2560
626.449.7650 (phone), 626.449.3536 (fax)
gene_ichinose@urscorp.com, hong_kie_thio@urscorp.com, paul_somerville@urscorp.com

NON-TECHNICAL ABSTRACT

The sources of seismic hazard in the Puget Sound Region of western Washington State is composed of Great M 9 earthquakes along the Cascadia subduction zone, along the interface between the Juan de Fuca plate and North America plate (e.g. the great earthquake which occurred in 1700), large shallow crustal earthquakes (e.g., from the Seattle and Whidbey Island faults), and deep (40 to 70 km) intraslab earthquakes. The last three intraslab earthquakes (1949 Olympia M=7.1, 1965 Seattle-Tacoma M_w=6.7, and 2001 Nisqually M_w=6.8) produced moderate levels of ground motions below 30% *g* (100% *g* is the acceleration experienced from the pull of gravity 9.81 m/s^2) yet caused widespread damage and disruption to buildings and transportation lifelines in the region. The frequent occurrence of these earthquakes makes it important to understand as much as possible about these events so that the hazard they pose can be more reliably quantified. An intraslab earthquake closer to urban Seattle or larger than the 2001 Nisqually earthquake can be expected to cause more damage than that from the Nisqually earthquake.

Our goal is to estimate the ground motions expected from a repeat of the 1965 Seattle-Tacoma earthquake near urban Seattle using new observations from recent earthquakes in 1999 and 2001. We accomplish this goal by applying a modeling method that includes the earthquake source (radiation pattern, directivity effects, spatial and temporal evolution of slip), realistic wave propagation effects, (reverberations, surface waves, and mode conversions), and amplification by site-effects based on surface geology and basin-depth effects. We use empirical data to validate the results. The ground motions for the Nisqually earthquake are displayed using a shake-map presentation. Shake-maps offer better portability to applications that use Geographic Information System technology such as HAZUS, developed by the Federal Emergency Management Agency to estimate the detailed losses sustained from natural hazards. We then apply the modeling method to estimate the ground motions experienced from the 1965 Seattle-Tacoma earthquake. The pattern of ground motions predicted for the 1965 Seattle-Tacoma earthquake is very different than those predicted for the 2001 Nisqually earthquake. These results predict that we can expect a severe level of shaking and moderate to heavy damage in the urban Seattle region (up to 60% g). Olympia and Everett are expected to experience only moderate levels around 10-20% g while Tacoma can expect accelerations of 30% g.

INTRODUCTION

Wadati-Benioff zone ("in-slab or intraslab") earthquakes occur frequently in the Puget Sound region of western Washington State (Figure 1). The 1946 Satsop (M 5.8-6.1) earthquake [Barksdale and Coombs, 1946] reoccurred in 1999 (M_w 5.7), the 1949 Olympia (M 7.1) earthquake [Nuttli, 1950; Baker and Langston, 1987] reoccurred in the Nisqually region in 2001 (M_w 6.7) [Ichinose et al., 2002]. Given the return time of 50 years for this pattern of in-slab earthquakes, we would expect the 1965 Seattle-Tacoma (M_w 6.7) earthquake [Langston and Blum, 1977], to reoccur in 2015. The return time of in-slab earthquakes is apparently every 30-50 years while the return time for crustal or subduction zone ("slab interface") earthquakes is every 300-1000 years. The more frequent in-slab earthquakes make it important to understand as much as possible about their source characteristics so that the hazard they pose can be more reliably quantified.

In-slab earthquakes, with hypocenters between 40 and 70 km depth, are presumably located within the upper part of the subducting Juan de Fuca plate [e.g., Kirby et al., 1996; Peacock and Wang, 1999]. The 2001 Nisqually earthquake produced only moderate ground motions below 0.3 *g* in the Puget Sound region. Nevertheless, these motions can be quite damaging where damage and widespread slope failures highlighted the vulnerability of buildings, lifelines, and transportation systems [Nisqually Earthquake Clearinghouse Group, 2001]. An earthquake slightly larger in magnitude or closer to urban Seattle could potentially cause more damage and disruption. This study examines the important question, "what ground-motions can be expected from a repeat of the 1965 Seattle-Tacoma event?"

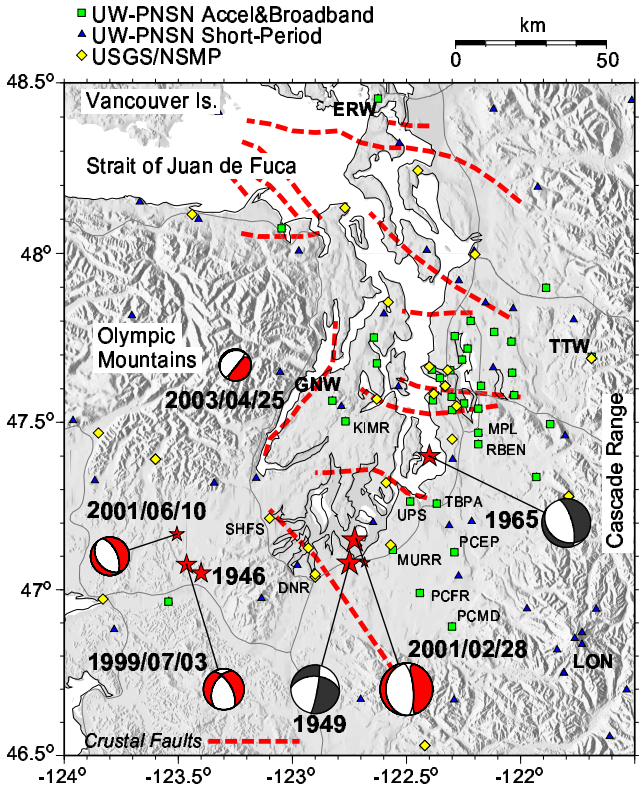

Figure 1. Location map of the 1999, 2001 Satsop, 2001 Nisqually, and 2003 Mount Olympus earthquakes including the locations of accelerometer and broadband seismic stations used in the finite-fault inversion. The focal mechanisms are determined using regional-wave moment tensor inversion. Also shown are the locations of historical 1946 Satsop, 1949 Olympia, and 1965 Seattle-Tacoma earthquakes.

New digital seismograms from the Nisqually and Satsop earthquakes allow for the reexamination of modern and historical Cascadia earthquake sources and ground motions. This study is also important because of the need to construct separate ground motion attenuation (GMA) models specific to the

Cascadia region [e.g., Crouse, 1991; Atkinson, 1995; Atkinson and Boore, 1997; Atkinson and Boore, 2003]. Past studies only included a few digitized records from the 1949 Olympia and 1965 Seattle-Tacoma earthquakes and also from recent Japanese and Mexico subduction zones. Currently available GMA models for Cascadia in-slab earthquakes are mostly based on a these global subduction zone databases, and are not in very good agreement with the ground motions recorded from the Nisqually earthquake. Recent analysis of global subduction zone earthquakes suggests interface earthquakes can produce ground motions greater than or similar to California crustal earthquakes for distances greater than 50 km [Youngs et al, 1997] because there was not enough data from in-slab earthquakes. Although the relationships are based in part on interface events, Youngs et al [1997] and Crouse [1991] indicate an increase in PGA and decrease in long-period S_a that suggests a higher stress drop of in-slab events. New high quality digital recordings from recent in-slab earthquakes, including the 2001 Nisqually and 1999 Satsop events, greatly increase the database of Pacific Northwest ground motion recordings.

APPROACH

We first invert long-period regional-waves to estimate the seismic moment tensor for the 1999 Satsop and 2001 Nisqually earthquakes. We then calibrate the Green's functions using a waveform inversion method on 3-component records at station Longmire (LON) to estimate a 1-D velocity model appropriate for ray paths crossing the Puget Sound. The inversion was performed on waveform data band-pass filtered between 0.05-1 Hz, appropriate for finite fault slip inversion. We then invert seismic and geodetic measurements to estimate the slip model for the 2001 Nisqually earthquake with a fault plane orientation assumed from the moment tensor and using Green's functions computed from the calibrated velocity model. We also invert teleseismic waves digitized from WWSSN records to estimate the slip model of the 1965 Seattle-Tacoma earthquake.

The 2001 Nisqually and 1965 Seattle-Tacoma slip models were used to generate ground motion time histories. A calibrated 1-D regional velocity model was used to compute Green's functions to frequencies of 10 Hz using f-κ summation and reflectivity method. The time-histories include the effects of directivity and radiation pattern for frequencies below 1-3 Hz. We then convolved a Kostrov shaped slip velocity pulse onto the Green's functions to include source controlled high frequency radiation ($f > 1$ Hz) predicted by dynamic rupture modeling [e.g., Miyake et al., 2001; Guatteri et al. 2002]. We also include a site amplification correction based on surface geology using a Quaternary, Tertiary, and Mesozoic (QTM) classification scheme [e.g., Park and Elrick, 1998, Wald et al., 1999] and amplification term based on basin depth (e.g., Field [2000] and Field [2001]). Modeling of the 2001 Nisqually earthquake ground motions was validated using observed PGA and S_a response spectra. We then performed simulations for a fine grid of receivers and applied site and basin-depth amplification corrections using interpolation to generate shake-maps of peak ground acceleration (PGA) and absolute acceleration (S_a) for the 2001 Nisqually and 1965 Seattle-Tacoma earthquakes.

COMPARISON WITH PREVIOUS EARTHQUAKE STUDIES

Several studies have examined the source parameters and ground motion characteristics from historical in-slab earthquakes. Langston and Blum [1977] inverted the WWSSN seismograms recorded at teleseismic distances for the point source parameters of the 1965 Seattle-Tacoma "Puget Sound" earthquake. They also performed a simultaneous determination of the crustal and upper-mantle structure. We used the faulting geometry and PS-9 velocity model [Langston and Blum, 1977; Burdick and Langston, 1977; Langston, 1977] to estimate the slip model in this study. The top of the subducting slab upper-mantle, and crustal structure has been constrained by many seismic studies [e.g., Langston, 1981; Owens et al., 1988; Weaver and Baker, 1988; Symons and Crosson, 1997].

Ihnen and Hadley [1986] generated a map of accelerations for the Puget Sound region from the 1965 Seattle-Tacoma earthquake using a combined three-dimensional ray tracing and WKBJ method. Absolute ground motions were not used by Ihnen and Hadley [1986] and instead they used a root mean square of

the accelerations scaled to fit an observed value at Tacoma. They also assume a point source for the earthquake. We used a mean ground motion value between both horizontal components and employ a finite-fault slip model that includes source radiation pattern and directivity effects. We do not include three-dimensional wave propagation but account for site and path effects using relationships from geology and basin depth with amplification. We also used an improved basin-depth map that is constrained using the Brocher et al. [2001] high-resolution tomographic inversion and SHIPS data.

Somerville and Smith [1991] simulated ground motions for the 1965 earthquake using a deterministic method similar in procedure to this study. They used some basic parameters estimated by Langston and Blum [1977] for a generic kinematic source description while this study uses a new improved slip model estimated from the inversion of the same teleseismic P- and SH-waves. Somerville and Smith [1991] used a generalized ray method to compute Green's functions that did not account for mode conversions, reverberations, and surface waves. They also assume an average radiation pattern.

SEISMIC AND GEODETIC DATA

We used broadband waveforms for the regional-wave moment tensor inversions of the Nisqually and Satsop earthquakes. We selected stations from the U. S. National Seismic Network operated by the U. S. Geological Survey (USGS), the Canadian National Seismic Network operated by the Geological Survey of Canada, and the Berkeley Digital Seismic Network operated by the University of California. We also included stations from Incorporated Research Institutions for Seismology (IRIS) regional and global networks. These stations were installed with Streckeisen STS1, STS2, or Guralp CMG-40 sensors. We added several local broadband stations from the Pacific Northwest Seismic Network (PNSN) operated by University of Washington for forward calculations.

The 2001 Nisqually and Satsop earthquakes were recorded by several networks of 3-component short-period, broad-band, and accelerometer seismic stations. We focused on complete seismograms that remained on-scale for the inversion of the slip models. A few stations were missing P-waves and pre-event due to late triggering and those records were only used for PGA and response spectra measurements. Figure 1 shows the location of PNSN accelerometers operated by the University of Washington, USGS National Strong Motion Network, and those operated by various local or state agencies (includes instruments K2, ETNA, Mt Whitney, SMA-1). We also included the dataset available from the Seattle Urban Seismic Array [Carver et al., 2001] that included Kinemetric K2's deployed by the USGS. All data are archived by the USGS National Strong Motion Project and made available to the public via the Consortium of Strong Motion Observation Systems (COSMOS) virtual data center. The seismograms from 12 stations labeled in Figure 1 were integrated to displacement to check near-field terms for the correct polarity. We later use the ground velocities from those stations in the slip inversion.

Teleseismic data for the Nisqually earthquake are archived by IRIS, which includes broadband stations from several global seismic networks. Teleseismic data for the 1965 Seattle-Tacoma earthquake were obtained from the Caltech film-chip library that archives microfiche from WWSSN stations operating between 1960 and 1980. The microfiche was printed and then scanned into a computer for manual digitization. Horizontal co-seismic displacements were recorded by Global Positioning System GPS satellites for the 2001 Nisqually earthquake. The processed GPS measurements were distributed by Central Washington University.

REGIONAL-WAVE MOMENT TENSOR INVERSION

We inverted the regional-waves for the moment tensor of four recent in-slab earthquakes (Table 1; Figure 1). We use the moment tensor methodology summarized by Jost and Herrmann [1989] following procedures similar to Ritsema and Lay [1995]. We band-pass filter the data and Green's functions between 200-20 second band for the Nisqually and 100-10 second waves for the Satsop earthquakes (Figure 2). Longer period waves are insensitive to the complexities from source-finiteness and path propagation effects. This assumption is appropriate when the dominant period of the waves, which have

wavelengths about 100 to 200 km in length, is much larger than the source dimensions or the dimensions of earth heterogeneities along the ray paths.

The Green's functions are computed using the reflectivity and frequency-wavenumber (f-κ) summation technique [Zeng and Anderson, 1995; Mueller 1985]. We computed the Green's functions using the WUS model (Table 2), constructed using phase velocity measurements of surface waves across the tectonically active regions of the western U. S. [Ritsema and Lay, 1995; Ichinose et al., 2003]. The receivers are distributed across different tectonic regions and therefore the choice of the velocity model used in the moment tensor inversion depends more on the site and path structure than on source structure.

Table 1. Regional-wave Moment Tensor Inversion Results

Date	Origin Time	Nodal Plane 1 Strike/Dip/Rake	Nodal Plane 2 Strike/Dip/Rake	M_o (dyne×cm)	M_w	Depth (km)	PDC[(1)]	Location
1999/07/03	01:43:55	206°/45°/-44°	330°/60°/-126°	4.81×10^{24}	5.72	40	98%	Satsop
2001/02/28	18:54:33	196°/22°/-67°	351°/68°/-98°	1.11×10^{26}	6.67	60	89%	Nisqually
2001/06/10	13:19:09	136°/34°/-106°	337°/58°/-80°	1.36×10^{23}	4.69	40	98%	Satsop
2003/04/25	10:02:13	252°/9°/-56°	38°/82°/-95°	6.76×10^{22}	4.49	46	79%	Mt Olympus

(1) Percent Double Couple

The waveform data are instrument corrected to displacement and then band-pass filtered. We use local network locations to compute a suite of Green's functions for 2 km depth increments and shift the data by increments of 1 second in origin-time. We then iteratively solve for the source depth and origin time using a grid search scheme to search for minima of the L2-norm objective function and maximize the percent double-couple of the moment tensor. We solve for the deviatoric moment tensor with 5 degrees of freedom. With only 5 degrees of freedom, we assume there is no volume change by replacing the moment tensor element M_{zz} with - (M_{xx}+M_{yy}). With a wide range of filter pass-bands and station distances, the inversion becomes heavily weighted toward higher frequencies and larger amplitudes from near-field stations. We do not apply distance weighting, although there is a natural weighting with distance because the farther stations usually have more data points. These complete waveform inversions are weighted more toward the surface than body waves because of the difference in amplitudes.

Table 2. Western U. S. (WUS) Velocity Model

Depth to top (km)	Thickness (km)	P-velocity (km/s)	S-velocity (km/s)	Density (g/cm^3)
0	4	4.52	2.61	2.39
4	28	6.21	3.59	2.76
32	20	7.73	4.34	3.22
52	∞	7.64	4.29	3.19

We used 7 stations (Figure 2A) in the moment tensor inversion for the 1999 Satsop earthquake. The centroid depth is 40 km and the origin time is 01 hrs, 43 min 55 sec. The grid search results and moment tensors varied little over a large depth range. Therefore we included station Longmire (LON) into the grid search to improve the resolution. The range of uncertainty in depth decreased to between 35 and 45 km and to within ± 1 second in origin time. The forward prediction at stations Tolt Reservoir (TTW) and Liberty (LTY) at higher frequencies validates the moment-tensor inversion and grid-search results.

We used 11 stations (Figure 2B) in the moment tensor inversion for the 2001 Nisqually earthquake. The centroid depth is 60 km and the origin time is 18 hrs 54 min 33 sec. The grid search results indicate very little change in the moment tensor and misfits for depths deeper than 60 km. The cross-correlation

between the data and synthetics is best between depths of 56 and 66 km. The waveforms from stations at Dodson Butte (DBO), Mount Erie (ERW), and Liberty (LTY) were left out of the inversion but used for prediction. The fits at these stations at higher frequencies are used as validation. We used 8 stations (Figure 2C) in the moment tensor inversion for the 2001 Satsop earthquake. The centroid depth is 40 km and the origin time is 13 hrs 19 min 09 sec. This event was very close in location and depth to the 1999 event (Figure 1). The range in uncertainty is 35 to 40 km and ± 1 second in origin time. We compared the predicted waveforms to the observations at stations Green Mountain (GNW), TTW, and Octopus Mountain (OCWA) to validate the results.

The depths of these four normal faulting earthquakes correlate closely with the top of the subducting Juan de Fuca plate indicating that they are intraslab (in-slab) resulting from localized tensile stresses within the plate. The stresses may be related to mineral phase transitions in the slab-crust from epidote-amphibolite to eclogite through a process of dehydration [Hacker et al, 2002; Dobson et al, 2002]. An alternative or contributing cause to the stresses may be related to a bend in the slab where the largest earthquakes in the Puget Sound and Strait of Georgia have occurred in historical and modern times.

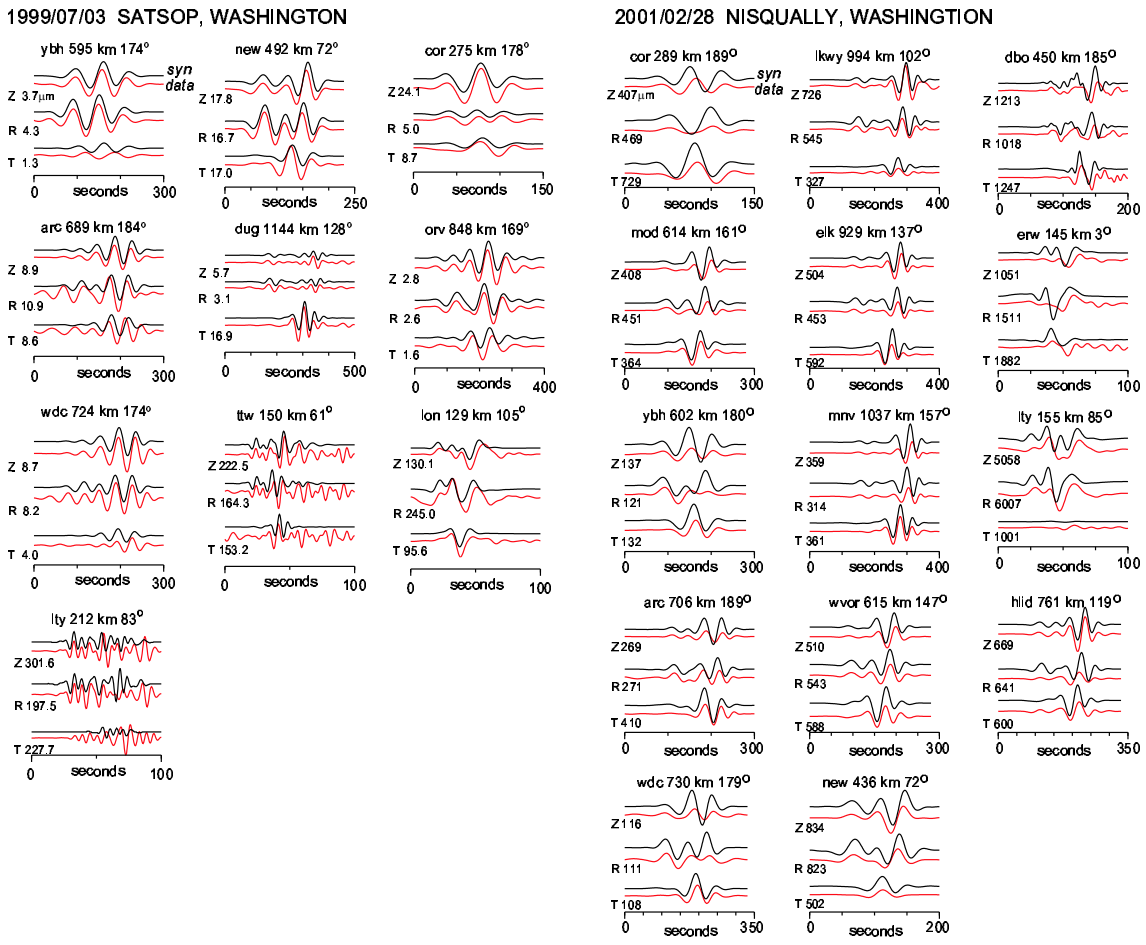

Figure 2. Regional-wave moment tensor inversion. Observed and predicted 3-component displacements for the (LEFT) 1999 Satsop (M_w 5.7) and (RIGHT) 2001 Nisqually (M_w 6.7) earthquakes. The station distance in km and azimuth in degrees from north are labeled above the waveforms. The amplitudes are in units of microns. The waveform data in red are plotted below the synthetics in black.

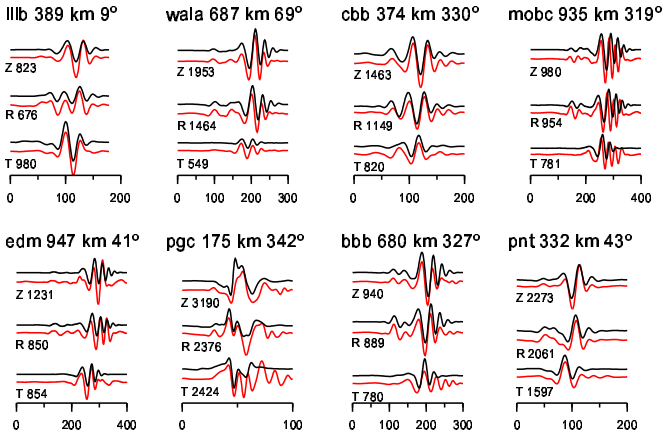

Figure 2 (continued). Observed and predicted 3-component displacements for the 2001 Nisqually earthquake (M_w 6.7). The station distance in km and azimuth in degrees from north are labeled above the waveforms. The amplitudes are in units of microns. The waveform data in red are plotted below the synthetics in black.

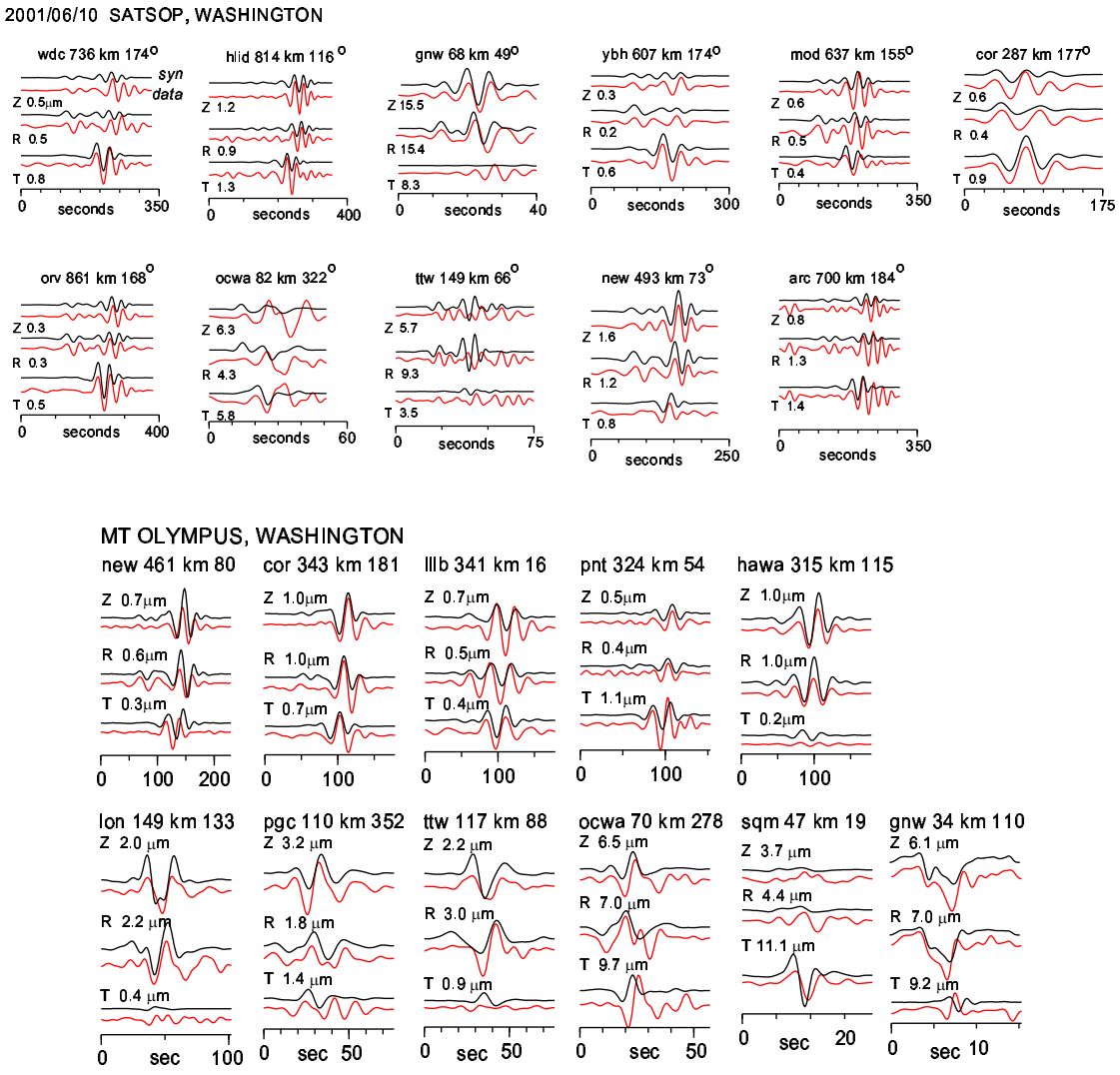

Figure 2 (continued). Observed and predicted 3-component displacements for the 2001 Satsop (M_w 4.7) and 2003 Mt. Olympus (M_w 4.5) earthquakes. The station distance in km and azimuth in degrees from north are labeled above the waveforms. The amplitudes are in units of microns. The waveform data in red are plotted below the synthetics in black.

GREEN'S FUNCTION CALIBRATION

We refined the one-dimensional velocity model used to compute Green's functions by minimizing the misfit between observed and synthetic seismograms using an iterative waveform inversion method similar to Xu and Wiens [1997]. We use shorter source and receiver distances and higher frequencies up to 1 Hz than their study. Calibrated Green's functions are important for the accurate estimation of moment tensors and slip models. Synthetic seismograms are computed from source parameters including the assumption of the earthquake location, source depth, scalar seismic moment, and focal mechanism. For this example, we use the location provided by University of Washington PNSN local short-period network and the long-period regional-wave moment tensor inversion result for the seismic moment and focal mechanism. The velocity model is parameterized as a stack of isotropic layers with P- and S-wave velocities and densities over a half-space. The earth layers have different thickness with thinner layers near the surface and thicker layers in the upper mantle and layers with equal thickness in the mid crust. A modified version of the PS-9 model [Langston and Blum, 1977] is used in this study as an initial model.

We applied the technique of Xu and Wiens [1997] for inverting waveforms to solve for the changes in earth velocities and densities. The i^{th} time point of the differential seismograms $\delta \boldsymbol{d}_i$ can be expressed as a system of linear equations of first-order partial derivatives ($\Delta \mathbf{G}_{ij}$) and first-order velocity perturbations ($\delta \boldsymbol{m}_j$) written as, $\delta \vec{\mathbf{d}}_i = \Delta \mathbf{G}_{ij} \delta \vec{\mathbf{m}}_j$ (Equation 1.), where the j^{th} layer of the velocity model is perturbed. The $m \times n$ matrix $\Delta \mathbf{G}_{ij}$ contains n columns of partial derivatives of the differential synthetic seismograms with respect to layer perturbations for each of the m perturbed layers in the velocity model. The m rows in $\Delta \mathbf{G}_{ij}$ are constructed by taking the two-point difference between the synthetics computed using the initial model and synthetics computed using the perturbed model. The differential seismograms are constructed by computing the two-point difference between the synthetics $\boldsymbol{s}_i$ computed from the initial model m^0_j from the observed seismogram ($\boldsymbol{d}_i$).

$$\delta \mathbf{d}_i = \mathbf{d}_i - \mathbf{s}_i(\mathbf{m}_j^{initial}) \qquad \text{(Equation 2. Differential Seismogram)}$$

$$\Delta \mathbf{G}_{ij} = \mathbf{s}_i(m_j^{perturbed}) - \mathbf{s}_i(\mathbf{m}_j^{initial}) \qquad \text{(Equation 3. Partial Derivative Matrix)}$$

Each j^{th} layer has a P-wave or S-wave velocity that can be perturbed from 1-10% from the initial model. We then invert matrix $\Delta \mathbf{G}_{ij}$ to form a set of normal equations,

$$\delta \mathbf{m}_j = \frac{\Delta \mathbf{G}_{ij}^{\mathbf{T}} \delta \mathbf{d}_i}{\Delta \mathbf{G}_{ij}^{\mathbf{T}} \Delta \mathbf{G}_{ij}} \qquad \text{(Equation 4.)}$$

where $^{\mathbf{T}}$ is the transpose operator. We then solve for j^{th} model layer perturbation $\delta \boldsymbol{m}_j$, which are the velocity and density changes required to fit the differential seismograms in a least squares sense. The inverse is performed using the conjugate gradient method [Claerbout, 1992] rather than by SVD or LU decomposition. The problem is nonlinear and its success depends on the proximity of the initial model to the true model. To overcome this non-linearity, we iterate the whole process by updating the initial model using the model perturbations and then solve for new model perturbations. Several (10-20) iterations are needed until there are either no significant improvements in the fit between data and synthetics or the fit worsens. The differential seismograms are computed using a fast reflectivity method [Zeng and Anderson, 1995]. We simplify the approach by assuming a fixed Poisson's ratio to get the P-wave velocities from the S-wave velocity. We also use a relation between density (ρ) and P-wave velocity (α), ($\rho = 0.32\alpha + 0.77$) [Berteussen, 1977].

We use records from the 2001 Satsop earthquake recorded at station Longmire (LON) to calibrate the Green's functions. The new velocity model is slower in the upper-crust relative to the PS-9 model (Table

3; Figure 3). The low-velocity zone between 40 and 60 km is inherited from the initial model and is probably poorly resolved. The new velocity model is used to generate synthetic seismograms at station LON and compared with the PS-9 model (Figure 3). Relative to PS-9, there are improvements in fitting the observed arrival time and amplitude of the SH-wave, arrival-times and amplitudes of the P-wave on the vertical and radial components, and the overall amplitudes for latter arrivals in the S-coda.

Table 3. New calibrated velocity model

Depth to Top(km)	Thickness (km)	P-velocity (km/s)	Q_p	S-velocity (km/s)	Q_s	Density (g/cm^3)
0	1.0	4.49	100.0	2.59	50.0	2.21
1	2.0	4.61	500.0	2.66	250.0	2.24
3	5.0	5.50	500.0	3.18	250.0	2.53
8	5.0	5.72	500.0	3.30	250.0	2.60
13	5.0	6.20	500.0	3.58	250.0	2.75
18	5.0	6.66	500.0	3.84	250.0	2.90
23	5.0	6.78	500.0	3.91	250.0	2.94
28	5.0	6.78	500.0	3.91	250.0	2.94
33	5.0	6.81	500.0	3.93	250.0	2.95
38	5.0	7.61	1000.0	4.39	500.0	3.20
43	5.0	6.57	500.0	3.79	250.0	2.87
48	5.0	6.57	500.0	3.79	250.0	2.87
53	5.0	7.53	1000.0	4.35	500.0	3.18
58	∞	7.68	1000.0	4.43	500.0	3.23

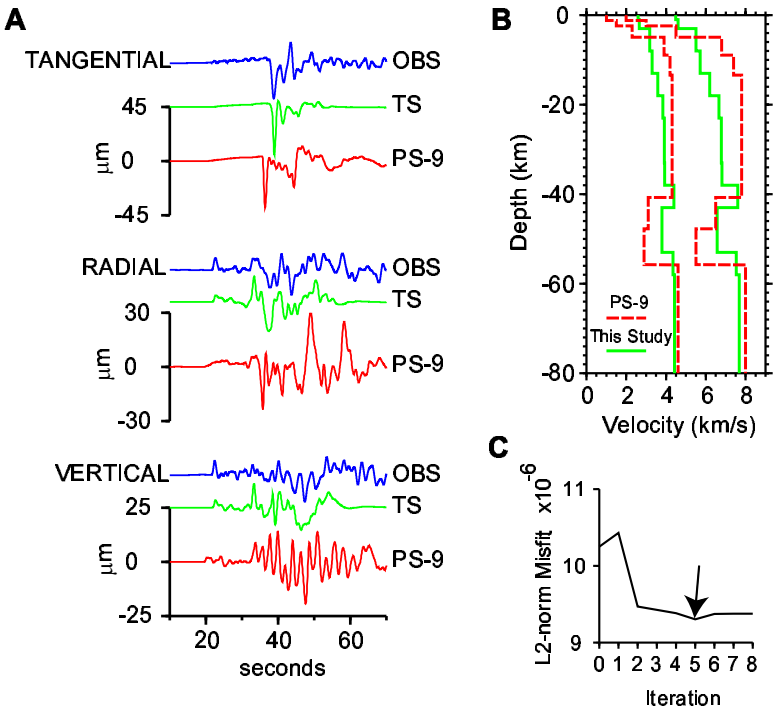

Figure 3. (**A**) Observed (*OBS*) ground displacements recorded at station Longmire (LON Δ=137 km ϕ=109°) from the 2001 Satsop, Washington earthquake (M_w 4.73, depth = 40 km) compared with synthetics computed using the (*PS-9*) velocity model and synthetics computed using a model developed in this study (*TS*). (**B**) The P-wave and S-wave velocity profiles show that the new model (*TS*) has lower velocities in the mid- and lower crust. The upper-mantle low-velocity zone is inherited from PS-9 velocity model. (**C**) The waveform inversion converged after 5 iterations

MULTIPLE TIME WINDOW INVERSION METHODOLOGY

We use local strong ground motion, teleseismic P- and SH-waves, and GPS horizontal co-seismic displacements, to invert the representation theorem for the spatial and temporal evolution of slip over the fault. The observed seismogram is related to the space and time integration of slip distributed across the fault plane **Σ** where,

$$U_n(\vec{x},t) = \int \partial\tau \iint \cdot \left[\cdot \left[\mu \cdot \vec{n}_i \cdot u_j(\vec{\xi},\tau) \right] \cdot G_{ni,j}(\vec{x},\vec{\xi},t-\tau) \right] \cdot \partial\Sigma \qquad \text{(Equation 5.)}$$

$U_n(\vec{x},t)$ is the n^{th} component of observed displacement. The term $\mu \cdot \vec{n}_i \cdot u_j(\vec{\xi},\tau)$ is a product of the rigidity, fault orientation vector, and fault slip at point $\vec{\xi}$ and time τ. $G_{ni,j}(\vec{x},\vec{\xi},t-\tau)$ is the Green's functions, that describes the wave propagation from each point on the fault to the receiver. x is the vector describing the relative location of the source and receiver. $\vec{\xi}$ and τ are the spatial and temporal variables of integration and i and j are orientations indices. The slip information $u_j(\vec{\xi},\tau)$ is to be determined by inverting the data.

We used a method for determining the slip distribution and history on a fault that was initially developed by Hartzell and Heaton [1983] called the multiple time window method [e.g., Wald and Heaton, 1994]. The fault plane is described by a grid of points for which Green's functions are computed for each grid to observation point. We then impose a propagating slip band, starting from the hypocenter that propagates over the fault plane at a fixed number of time steps. The slip band is characterized by two parameters. The first parameter is the rupture velocity, which is the maximum velocity of the rupture front (v_{rup}), and second is the maximum dislocation rise time (T_r), which expresses the maximum duration of slip allowed at a grid point after the passage of the rupture front.

The individual sets of grid points that are contained within a slip band, at each time step, are combined and cast into a set of normal equations of the form: $\mathbf{A}\underline{x} = \underline{b}$, where **A** contains the Green's functions from every grid point to every station, $\underline{x}$ is the solution vector containing the slip value at every grid point, and $\underline{b}$ is the vector containing all the data [Lawson and Hanson, 1974]. The normal equations for each time step are combined and then solved simultaneously using a linear least squares solver with a positivity constraint thereby preventing back-slip. This method allows for variable rake, in which every original grid point is split into two where the new rake angles are different from the original by ±45°.

This inverse problem has many degrees of freedom, so we applied some regularization of the normal equation to prevent strongly oscillating solutions. We applied spatial smoothing constraints as well as smoothing of the two perpendicular rake vectors. Strong smoothing of the rake vectors forces the two vectors to have equal amplitudes and thus revert to the original rake angle. The smoothing operations are included by adding terms of the form, $\mathbf{A}' = \gamma \cdot \mathbf{I} \cdot (1-\lambda)$, (Eq. 6) where, **I** is the identity matrix, γ is the damping parameter and λ is the smoothing parameter. The **A**' matrix is appended to the bottom of the matrix **A** and adding a zero to the bottom of vector $\underline{b}$ for every added row to matrix **A**.

With a diverse dataset, it becomes necessary to impose a weighting scheme in order to ensure that some data do not dominate other data in the inversion. This is a controversial issue, since errors associated with certain types of data can be quite different from others. Also, in the least squares inversion, it is important to take into account the number of data points per record, as well as the absolute amplitude of the data. On the other hand, seismic data can sometimes have a nodal character and be more susceptible to contamination from scattering. Between different types of data sets there are also large differences in absolute amplitude. Therefore, we used a weighting scheme that uses overall weight per data type, and within each group an automatic weighting based on the absolute amplitude and number of points, following an empirically derived equation,

$$w = \frac{\alpha \log(a_{\max})}{n a_{\max}} \qquad \text{(Equation 7.)}$$

where w is the weight, α the overall weight for this particular data type, $a_{\max}$ the maximum amplitude of the record, and n the number of points per record. From experience, this weighting scheme gives good results and is rather efficient since it only requires the overall weighting factor a to be specified. Many of the inversion parameters such as smoothing and data type weighting parameters are determined by trial and error.

The teleseismic Green's functions are computed using a propagator matrix algorithm for the effects of near source and receiver structure and simple teleseismic ray corrections for the mantle part of the rays. Attenuation is included using the t^* operator with values of 1 and 4 for P and S-waves respectively [*Langston and Helmberger*, 1975]. Velocity models are required for the source, receiver, and bounce point regions.

FINITE FAULT SLIP MODEL: 1965 Seattle-Tacoma Earthquake

We inverted 32 teleseismic P- and SH-waves recorded by the WWSSN for the slip and variable rake of the 1965 Seattle-Tacoma earthquake (Figure 5 and 6) using the multiple time window method. We assume the geometry for the fault model based on the focal mechanism estimated from Langston and Blum [1977] teleseismic point source modeling for computing the Green's functions (Figure 4). The fault is parameterized as a planar surface subdivided into 150 grid points with grid spacing of 2×2 km. The dimension of the rupture plane along strike is 30 km and along dip is 20 km. The fault strike is fixed at 344°, the fault dip is fixed at 70°, and although the rake is estimated to be -75°, it is allowed to vary in the inversion from -45° to -135°. The top and bottom edge of the fault have depths of 52 and 70 km. The coordinate of the southwest corner is 47.26°N, 122.29°W. We use the location of 47.397°N, 122.310°W, and 60.5 km depth, for the start of the rupture. The PS-9 velocity model is used to compute the teleseismic Green's functions using the Generalized Ray Method. The two horizontal components were digitized and aligned along the P-wave arrival before rotation into SV- and SH-wave components. The WWSSN instrument response was convolved onto the Green's functions to avoid instabilities that may result from instrument response deconvolution on digitized data.

The rupture is parameterized as 6 time windows spaced at 1-second intervals and a rupture velocity of 3.2 km/s. The maximum dislocation rise time is 3 seconds and the source time function at each grid point is a triangle with 1-second rise and 1-second fall-off. We selected a maximum rise time based on the inspection of spectra from 2001 Nisqually earthquake strong ground motion records, which suggested a rise time between 1 and 3 seconds. The minimum rise time for crustal earthquakes ranges from 0.6 sec [Heaton, 1990] to 0.9 sec according to empirical relations of Somerville et al. [1999]. Asano et al. [2003] suggest that this rise time is 0.12-0.24 sec for Japanese in-slab earthquakes.

The slip model has two small asperities of about 4 and 8 km^2 in area 2 km up-dip and 4 km south of the hypocenter. The maximum of slip of first asperity is 2 meters and the second asperity is 2.8 meters and the total seismic moment is 9.43×10^{25} dyne×cm (M_w 6.63). The scalar moment is similar to that estimated by Langston and Blum [1977], although their total slip duration was only 3 seconds.

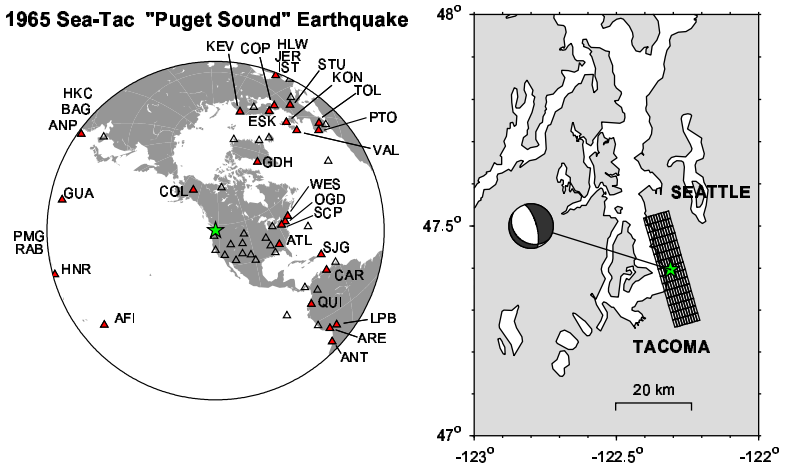

Figure 4. Teleseismic station map and source grid for the 1965 Seattle-Tacoma earthquake.

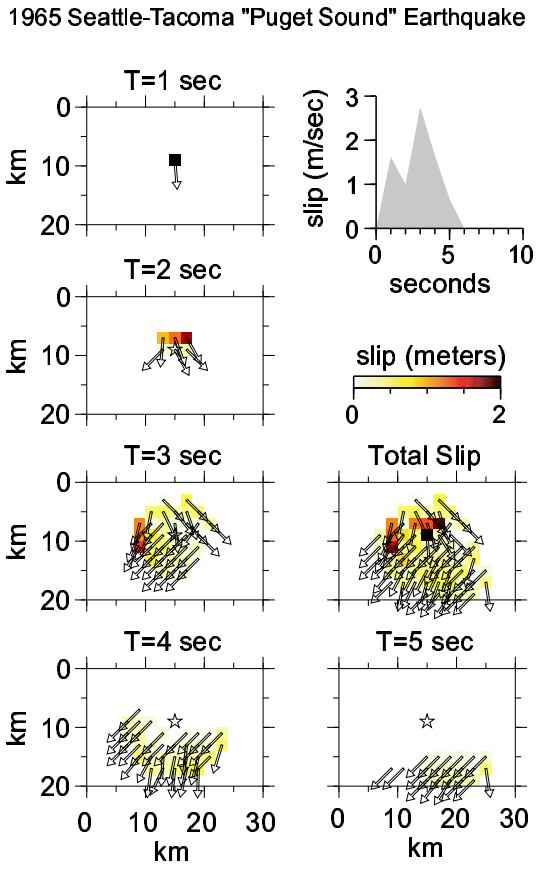

Figure 5. (left) 1965 Seattle-Tacoma slip inversion results.

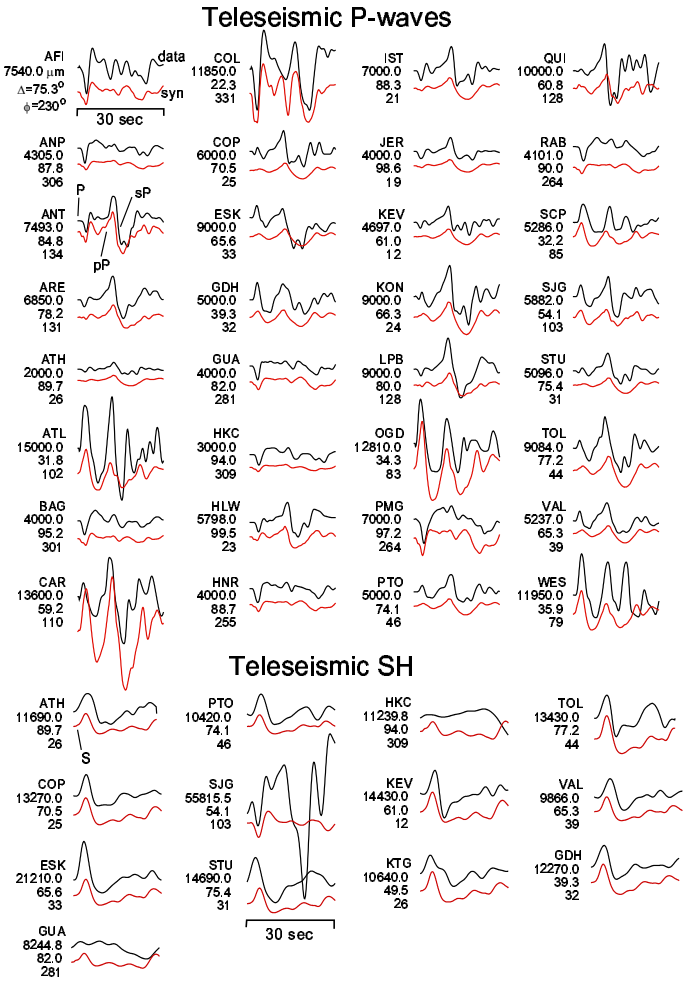

Figure 6. (right) Predicted and observed teleseismic waveforms.

FINITE FAULT SLIP MODEL: 2001 Nisqually Earthquake

We inverted strong ground motion, teleseismic body waves, and coseismic displacements for the slip model of the 2001 Nisqually earthquake using the multiple time window method. The fault is parameterized as a planar surface divided into 80 grid points with grid spacing of 3×3 km. The dimension of the rupture plane along strike is 30 km and along dip is 24 km. We assume the steeply dipping fault plane geometry for the fault model based on the focal mechanism estimated from the regional-wave moment tensor inversion for computing the teleseismic Green's functions (Figure 7). There is an ambiguity of the rupture plane between the two nodal planes and the geodetic or teleseismic data alone does not appear to resolve the fault plane ambiguity. The fault strike is fixed at 355°, the fault dip is fixed at 70°, and the rake is allowed to vary in the inversion from -45° to -135°. The top and bottom edge of the fault have depths of 45 and 67 km. The coordinate of the southwest corner is 47.015°N, 122.730°E. We use the location of 47.139°N, 122.705°W, and 55 km depth, for the start of the rupture.

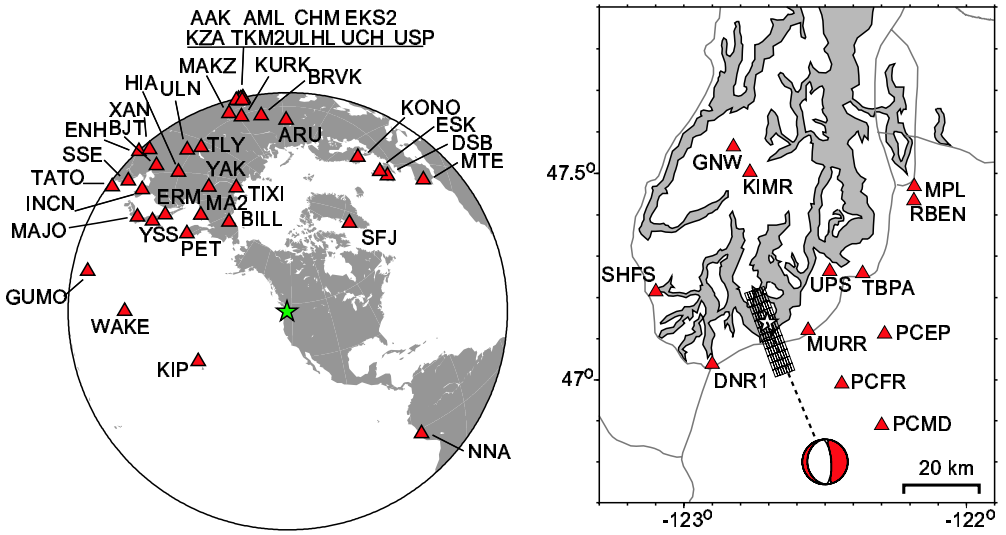

Figure 7. Teleseismic station locations, local accelerometer stations, and finite-fault source grid.

We performed a slip inversion of 12 local strong ground motion, 30 teleseismic P-waves, 7 teleseismic SH-waves, and horizontal co-seismic displacements from 8 GPS stations for the rupture history of the 2001 Nisqually earthquake. Acceleration waveforms were integrated to velocity and low-pass filtered at 0.5 Hz while the teleseismic waveforms were instrument corrected to displacement without filtering. We use the PS-9 model to compute the teleseismic Green's functions, and the new calibrated model to compute the local strong ground motions. The Green's functions for the co-seismic displacements were calculated using an elastic half-space with the equations of Okada [1992]. Rupture is assumed to initiate at the hypocenter at 56 km depth, estimated by the University of Washington PNSN using P-phases from their short-period seismic network (Figure 8). The maximum rupture velocity is set to 3.2 km/sec and we use 6 time windows at 1-sec intervals. We assume a maximum dislocation rise time of 3 sec. An inversion using a maximum rise time of 1 sec did not change the rupture history results.

The slip model consists of a small 12 km^2 area centered 3 to 6 km down-dip from the hypocenter (centroid of seismic moment release is between 59-62 km), which is consistent with regional-wave moment tensor inversion results. The seismic moment is 1.59×10^{26} dyne×cm (M_w 6.74). The greatest amount of slip (3.35 m) is located at the hypocenter with most of rupture down-dip and elongated in the north-south (along strike) direction (Figure 8).

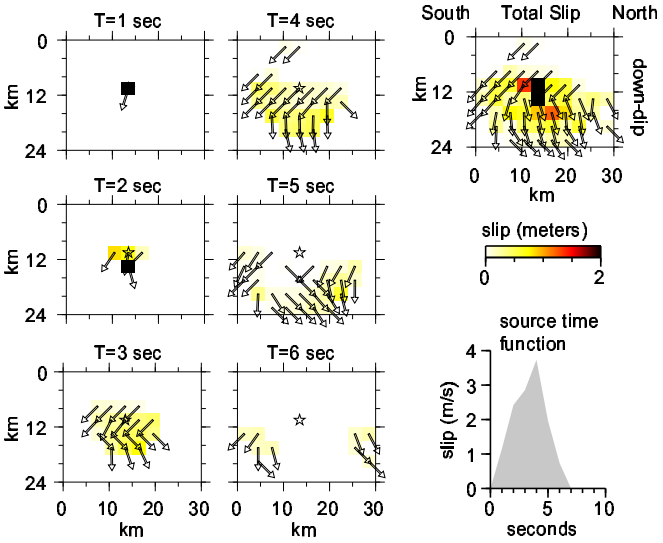

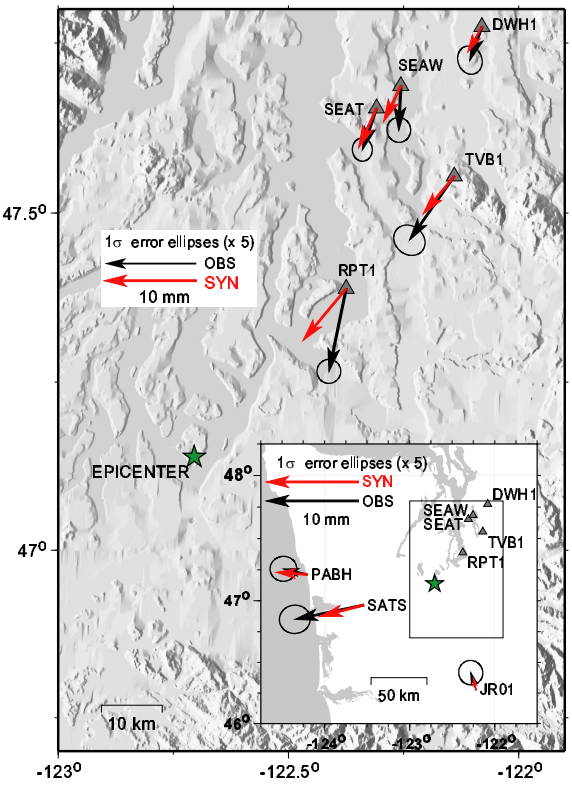

Figure 8. 2001 Nisqually slip inversion results.

Figure 9. GPS horizontal Co-seismic Displacements

The horizontal co-seismic displacements from GPS receivers were not weighted highly in the slip inversion (Figure 9). Initial tests indicate a discrepancy with conflicting measurements at sites RPT1 and SEAW compared to the whole GPS dataset. There is no combination of fault orientations, source depths or locations which can exactly fit all of the horizontal displacements and without these two receivers, a smoothed inversion of only GPS data resulted in a region of slip just southeast of the hypocenter. We speculate that the measurements at RPT1 and SEAW may be affected by monument stability problems perhaps by soil liquefication. A separate analysis of GPS data by R. McCaffrey (Rensselaer Polytechnic Institute, New York) estimates a seismic moment of 1.4×10^{26} dyne×cm (M_w 6.7) consistent with regional moment tensor inversion results ($M_o=1.11\times10^{26}$ dyne×cm) and slip-model inversion ($M_o=1.59\times10^{26}$ dyne×cm). Their average slip of 0.98 meters is consistent with 1.3 meters using a similar fault area and average slip. Their depth of 61 km is also consistent with that estimated by regional moment tensor inversion (60 km).

Teleseismic records between the 1965 Seattle-Tacoma (Figure 6) and 2001 Nisqually (Figure 10) earthquakes appear similar indicating the same faulting geometry. The long-period response (10-30 seconds) of WWSSN instruments makes a detailed comparison difficult yet some information can be extracted. For instance, at stations (KONO,KON) and ESK the relative P-pP amplitudes indicates a slight change in focal mechanism.

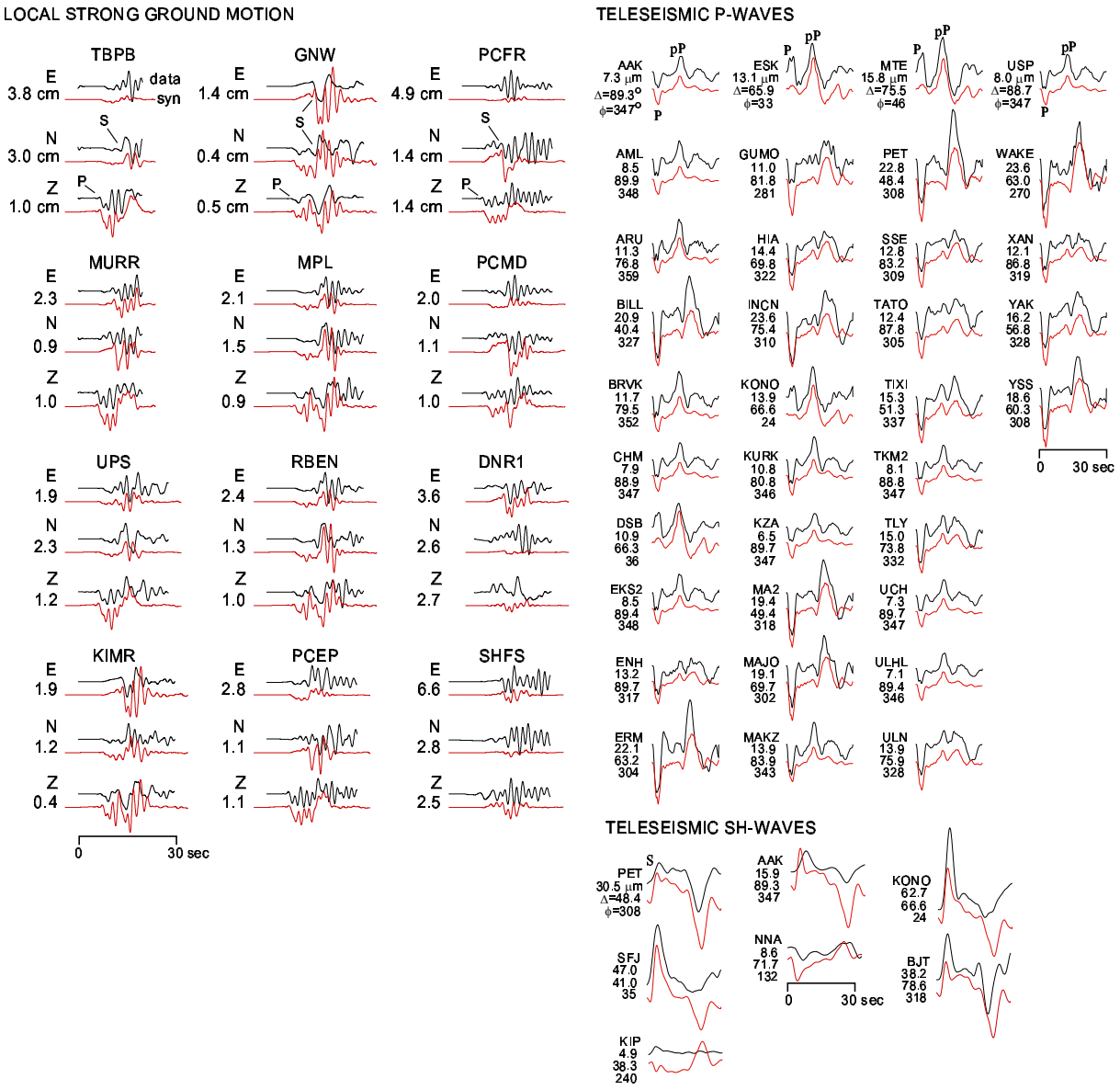

Figure 10. Comparison between observed and synthetic strong ground motions and teleseismic P- and SH-waves.

SHAKE-MAP SIMULATION METHODOLOGY

The most important information for emergency response personnel and engineers, after earthquake location and magnitude, is the assessment of damaging near-fault strong ground motions [e.g., Wald et al., 1999; Dreger and Kaverina, 2000]. The goal here is to apply a time-domain based modeling method that uses the spatial and temporal evolution of slip, surface geology as a proxy for site amplification, and basin amplification function to estimate the ground motion levels for the 1965 Seattle-Tacoma and 2001 Nisqually earthquakes. We test these predicted ground motions with those observed in the Nisqually earthquake. We then apply this modeling method to estimate the ground motions experienced from the 1965 Seattle-Tacoma earthquake, which is important for preparing for an expected future in-slab

earthquakes near urban Seattle. The reexamination of an historical earthquake using an empirically derived slip model adds more realism than a randomly derived slip model for a scenario earthquake. The shake-maps will show peak horizontal acceleration (PGA) and the 5% damped absolute acceleration (S_a) at periods of 0.3, 1, and 3 seconds. Shake-maps offer better portability to applications that use Geographic Information System technology such as Hazards U. S. (HAZUS), the government and industry standard software application developed by the Federal Emergency Management Agency to estimate the losses sustained from natural hazards.

We use a time-domain approach to generate time-histories for creating shake-maps. The fault is subdivided into 1×1 km elements and Green's functions are computed from each element to a grid of receivers using the reflectivity method with a 1-D velocity model (Table 3; Figure 3). The Green's functions are lagged and summed based on the slip function. The resulting synthetics include the effects of source radiation pattern, directivity, and 1D wave propagation effects (e.g., mode conversions, reverberations, and surface waves). Ground motions are computed for a grid of receivers spaced approximately 10×10 km. About 60,000 Green's functions were computed using the *f*-κ reflectivity method, taking 2 days on a 1.7 GHz Intel P-4 processor workstation. The peak motions from simulated acceleration time histories and response spectra are averaged between the horizontal components, then spatially interpolated using a bicubic scheme to form a map with a grid spacing of 100×100 meters.

The method lacks accuracy at higher frequencies (f > 1-3 Hz) due to the assumption of the triangle shaped slip velocity time function. This function describes the slip of a grid point for any single time-step and is convolved with the Green's functions before lagging and summation process. Miyake et al. [2001] proposed using a Kostrov type slip velocity time function to simulate broadband ground motions. Figure 12 compares the Fourier amplitude spectrum for the triangle function with the Kostrov function. The triangle has holes in the high frequency spectrum while the Kostrov is a better replication of the ω^{-2} source spectrum. We therefore replace the triangle function with the Kostrov function for each source element. The Kostrov shape for the slip velocity time function is observed from the dynamic simulations of earthquakes using fracture energy and stress drop as spatial random fields [e.g., Guatteari et al. 2003].

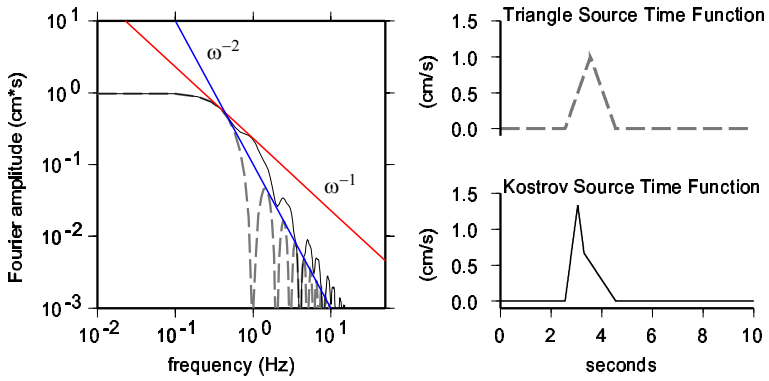

Figure 12. Comparison between Triangle and Kostrov shape source-time functions.

The ground motions are computed for the region using a grid spacing of approximately 10×10 km, interpolated using a bicubic scheme [Wessel and Smith, 1991], and then corrected for site effects using surface geology as a proxy for V_s^{30}, the shear wave velocity for the upper 30 meters, and basin depth [e.g., Field, 2001]. We use a Quaternary, Tertiary, and Mesozoic (QTM) classification scheme developed by Wald et al. [1999]. Figure 13 shows a geologic map of the Puget Sound and surrounding regions of western Washington State compiled by Schuster [2002]. The geologic units are digitized as polygons and we use a program that determines the QTM geologic identification given a map position. A map of QTM

classification was constructed for the same 2°×2° region with a grid spacing of about 100×100 m. The amplification is a function of QTM, level of ground motion (PGA or S_a), and frequency or period. We use the Park and Elrick [1998] and Wald et al. [1999] relationships to develop equations for amplification as a function of ground motion. These relationships are found for each QTM classification and period in Table 4.

Table 4. Site Amplification

Geology (V_s^{30})	Amplification Factor [1]	Period – T (seconds)
Quaternary (333 m/s)	Amp = 1.52 – 0.57 ζ	T >= 1.0 seconds
	Amp = 1.31 – 0.84 ζ	T < 1.0 seconds & PGA
Tertiary (406 m/s)	Amp = 1.32 – 0.33 ζ	T >= 1.0 seconds
	Amp = 1.21 – 0.57 ζ	T < 1.0 seconds & PGA
Mesozoic (589 m/s)	Amp = 1	

[1] ζ = ground motion (e.g., PGA or S_a)

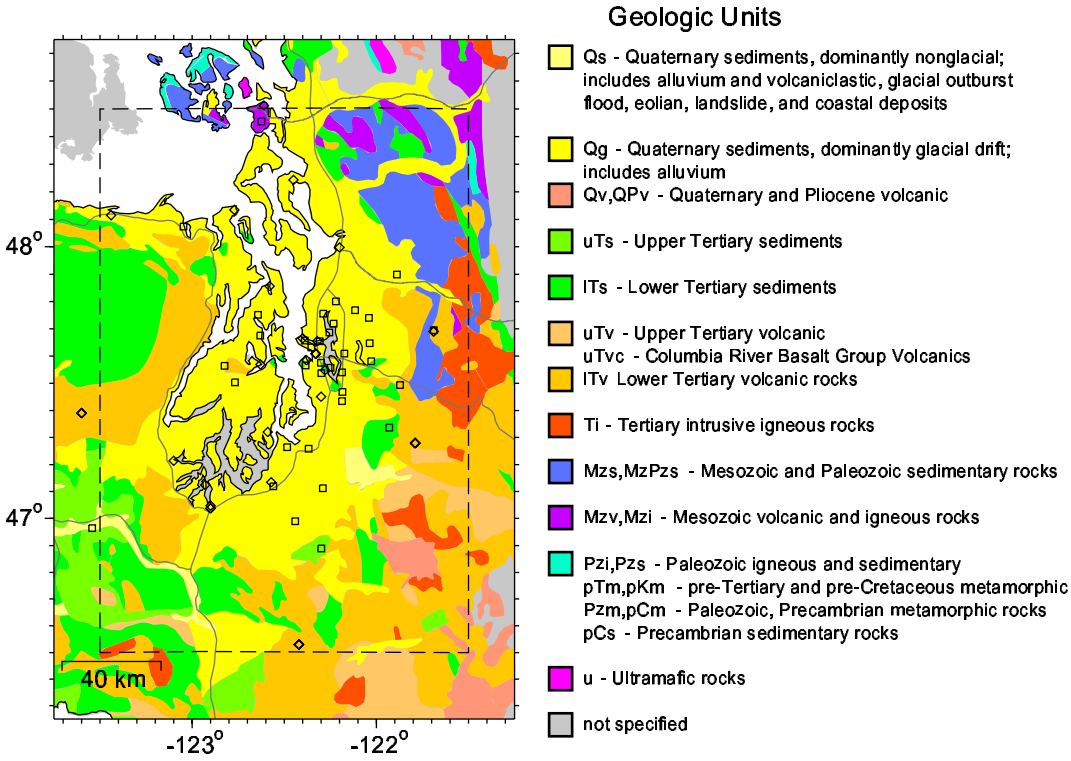

Figure 14. Geologic map of the Puget Sound region. The dashed box includes the region of the shake-map calculation. Squares and diamonds are the locations of accelerometer sites.

The other modification is for basin depth effect. The basin depth was estimated for the Seattle, Tacoma, and Everett basins by Brocher et al [2001] using high resolution seismic tomography from the SHIPS experiment. We did not include the Tacoma basin in the southern portion of the Puget Sound due to incomplete information. The sediment thickness there could be as deep as 5 km while it is as deep as

5.5 and 8 km in the Everett and Seattle basins respectively. We digitized the sediment thickness map by Brocher et al [2001] for the Seattle and Everett basins. The depth contours were digitized at 0.5 km intervals as polygons and we use the same program which identifies geologic polygons to identify these polygons as depth contours. From this program we constructed a basin depth map for a grid of points with 100×100 m spacing shown in Figure 14. These basins have P-wave velocities ranging from 1 km/s to 4.5 km/s, with the basin thickness defined as the 4.5 km/s P-wave or approximately 2.6 km/s shear-wave velocity isosurface. We use a relationship $Amplification = \exp(0.12 \cdot h)$ where h is the basin depth, derived from empirical southern California ground motions by Field [2000; 2001] for 1-second spectral acceleration. The sediment bedrock interface is defined in this relationship by the 2.5 km/s S-wave velocity isosurface for the southern California velocity model. The calibrated Puget Sound model also has a consistent surface S-wave velocity of 2.5 km/s.

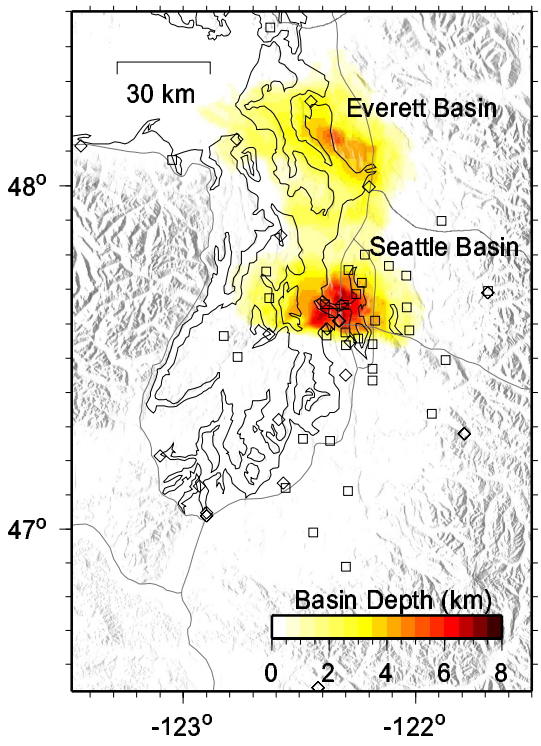

Figure 14. Basin depth map.

OBSERVED AND SIMULATED GROUND MOTIONS

We assess the performance of current ground motion models (PGA and S_a) [e.g., Crouse, 1991; Somerville and Smith, 1991; Youngs, et al. 1997; Atkinson and Boore, 1997; Atkinson and Boore, 2003], for in-slab Cascadia earthquakes using the 2001 Nisqually ground motion datasets. The x-axis is the closest distance to the fault plane calculated using the finite-fault grid (Figure 7). The y-axis is the free-field or basement peak horizontal ground motion from either the north-south or east-west component. Previous GMA models and relationships perform well between distances of 50 and 100 km and slightly over predict at distances between 100 and 200 km (Figure 15). There are no distances below 50 km because of the depth of in-slab earthquakes. The recorded horizontal PGA are mostly scattered below the Youngs et al [1997] soil and above the Atkinson and Boore [1997] GMA models.

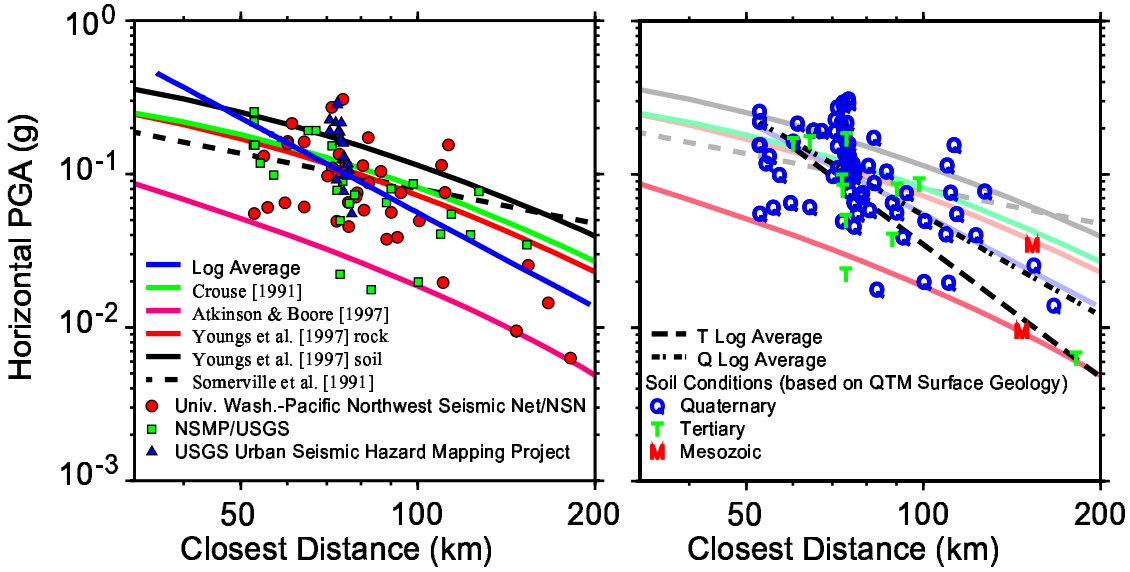

Figure 15. Horizontal PGA observed from the 2001 Nisqually earthquake categorized by seismic network and site geology using the QTM classification scheme.

We estimate a log average type ground motion attenuation model using the simple functional form, *log*(PGA) = *a* + *b log*(R), where R is the closest distance to the fault, *a* is the y-axis intercept coefficient, and *b* is the slope coefficient. These coefficients and their probable uncertainties σ_a and σ_b, are estimated using a least squares inverse. We also analyze any bias or spread in the residuals by calculating their standard distribution σ_r (Table 5). These coefficients are applicable between the ranges of 50-200 km.

Table 5. PGA attenuation coefficients, uncertainties, and standard deviations

Data-set	*n*	*a*	*b*	σ_a	σ_b	σ_r
All sites	89	6.46	-2.03	1.06	0.24	0.066
Quaternary sites	89	7.10	-2.18	0.74	0.17	0.065
Tertiary sites	89	9.80	-2.86	0.40	0.078	0.014
Simulation	183	6.26	-2.00	0.85	0.19	0.10

The log average of the observed PGA data is most similar to the Crouse [1991], Somerville and Smith [1991], and Youngs et al. [1997] rock GMA models. We separate the PGA based on site geology using the QTM classification scheme. Most of the PGA are measured at sites with Quaternary geology and therefore the log average of the Quaternary PGA is similar to that of the entire dataset (Table 5; Figure 15). The log average of the PGA on Quaternary compared to Tertiary surface geology is similar at 50 to 60 km with a significant increase in the decay at farther distances. The change in slope between Quaternary and Tertiary sites is 0.68, which is more than three times larger than the probable uncertainties in σ_b (0.17 and 0.078) for both types of sites (Table 5).

We implement the previously described scheme to simulate ground motion time histories using the finite-fault slip model of the 2001 Nisqually earthquake. These are corrected for surface geology and basin depth. The spectra of the 5% damped absolute accelerations (S_a) for the two horizontal components at 60 sites are shown in Appendix A1 along with the site classification and basin depth beneath the site.

The simulated spectra fit the observed spectra except for east-west oriented components at several stations near the Seattle basin. We will further examine these ground motions in a later section.

Figure 16 shows the simulated PGA from the 2001 Nisqually earthquake, corrected for site and basin depth effects, compared with GMA models from various studies of global interface and in-slab earthquakes. The differences between the coefficients *a* and *b*, estimated from simulated and observed PGA (Table 5) are much smaller than their probable uncertainties. The standard deviations of their residuals are also similar. This similarity between the log average and distribution of the simulated and recorded PGA suggest that PGA can be estimated fairly well using this method.

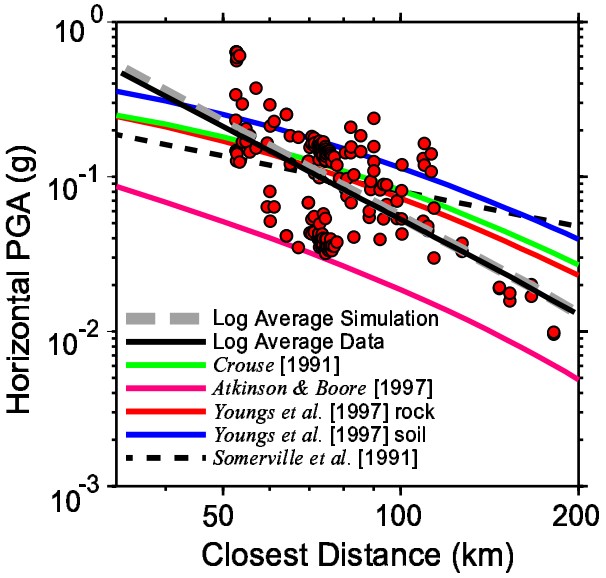

Figure 16. Predicted horizontal PGA for the 2001 Nisqually earthquake. The log average of the recorded PGA is consistent with the log average of the predicted PGA.

Figure 17 shows the predicted S_a at T=3, 1, and 0.3 seconds for the 2001 Nisqually earthquake compared with observations and GMA models from previous studies. These response spectral values are calculated for a single degree of freedom oscillator with 5% damping. The simulation for the Nisqually earthquake predicts the observed S_a values reasonably well at 1 and 0.3 seconds and have very similar log average relationships (Table 6). The predicted and observed Sa values mostly lie below the GMA models for Youngs et al [1997] on soil and above the Atkinson and Boore [1997] for T=1 and 0.3 seconds and above Youngs et al [1997] for rock for T=3 seconds.

Table 6. S_a attenuation coefficients, uncertainties, and standard deviations

Data-set	*T*	*n*	*a*	*b*	σ_r
Observed	0.3	66	6.69	-2.01	0.22
Simulated	0.3	282	6.83	-2.11	0.10
Observed	1.0	66	5.83	-1.99	0.086
Simulated	1.0	282	5.09	-1.91	0.028
Observed	3.0	66	5.13	-2.30	0.010
Simulated	3.0	282	-2.13	-0.63	0.005

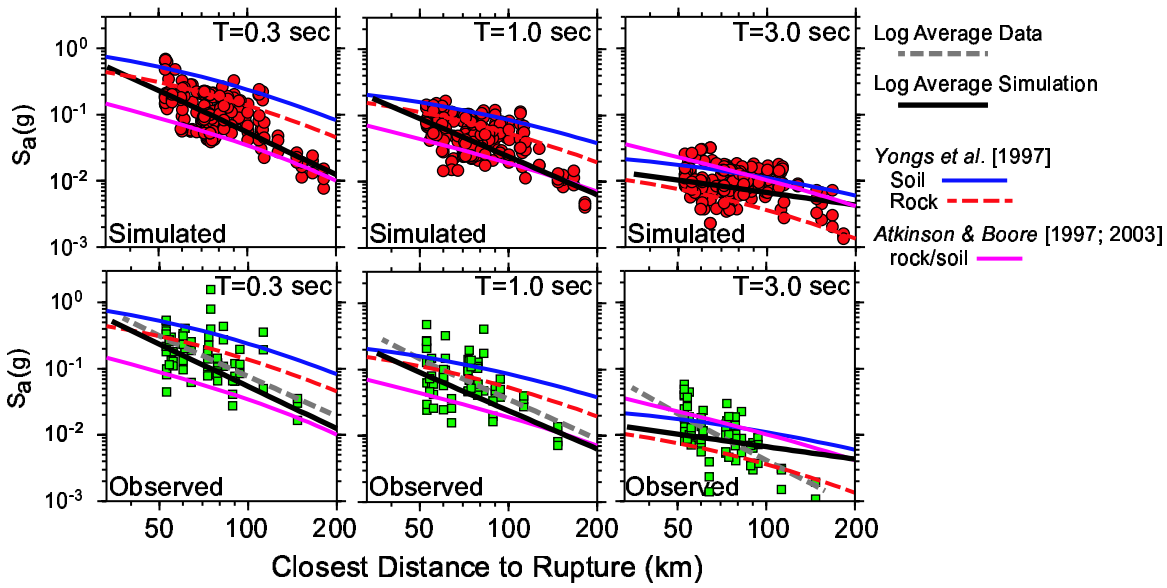

Figure 17. Observed and simulated absolute acceleration response spectral levels at 3, 1, and 0.3 seconds period. The absolute acceleration is slightly under predicted at short periods.

We examined the residuals between the recorded and simulated ground motions (PGA and S_a) with and without site geology and basin-depth corrections. The effect of the corrections on residuals is to remove the biases (mostly under predicted bias) on the distribution of residuals but not decrease the spread of the residuals. This is illustrated in Table 7, that shows for PGA and S_a at T=0.3 sec and T=1.0 sec. The median of the residuals from the uncorrected ground motion levels are decreased toward zero but the standard deviations remain the same. The exception is with S_a at T=3.0 seconds where it appears that the site and basin-depth effects are not as significant at longer periods. We will provide an explanation for this in the discussion section.

Table 7. Median and standard deviation of corrected and uncorrected ground motion residuals

	Uncorrected μ	*Corrected* μ	*Uncorrected* σ	*Corrected* σ
PGA	0.028	-0.013	0.078	0.083
S_a T=0.3	0.11	0.04	0.19	0.20
S_a T=1.0	0.058	0.017	0.098	0.096
S_a T=3.0	-0.021	-0.031	0.036	0.057

μ – median, σ - standard deviation

We noticed an interesting correlation between the ground motion residuals and the distance of those ground motions from the Seattle fault not observed when plotted from the epicenter. Figure 18 shows these residuals versus distance from the surface trace of the Seattle fault and 2001 Nisqually earthquake epicenter. The figure shows the distribution of these residual for both corrected and uncorrected ground motions. We see that most ground motion levels, except for S_a at 3 seconds, are under predicted near the surface trace of the Seattle fault. This is not observed when the ground motions are plotted from the epicenter. Amplification factors between 2 and 5 for frequencies below 5 Hz were estimated for sites in urban Seattle and the Duwamish Valley by Frankel et al [1999] and Hartzell et al [2000]. Modeling using

1- and 2-dimensional modeling suggests some of the amplifications were attributed to basin edge effects.

This effect is better quantified using the linear correlation coefficient r and significance level Ψ. Table 8 illustrates that r is two or three times larger when the residuals are plotted from the Seattle fault than from the epicenter. The smaller Ψ's indicate that these have a more significant correlation. The application of the corrections removes this correlation. The residuals, relative to the epicenter, do not show any significant correlations before or after the corrections. This indicates that the higher correlation of the uncorrected residuals (or under predicted ground motions) may be due to a 3-D basin edge effect from the truncation of subsurface sediments by the Seattle fault. This effect is similar to that modeled by Graves et al., [1998] observed in Santa Monica, California from the Northridge earthquake. The removal of the correlation and bias after the correction suggests that the basin depth of Field et al [2000; 2001] is somewhat applicable to the Puget Sound region.

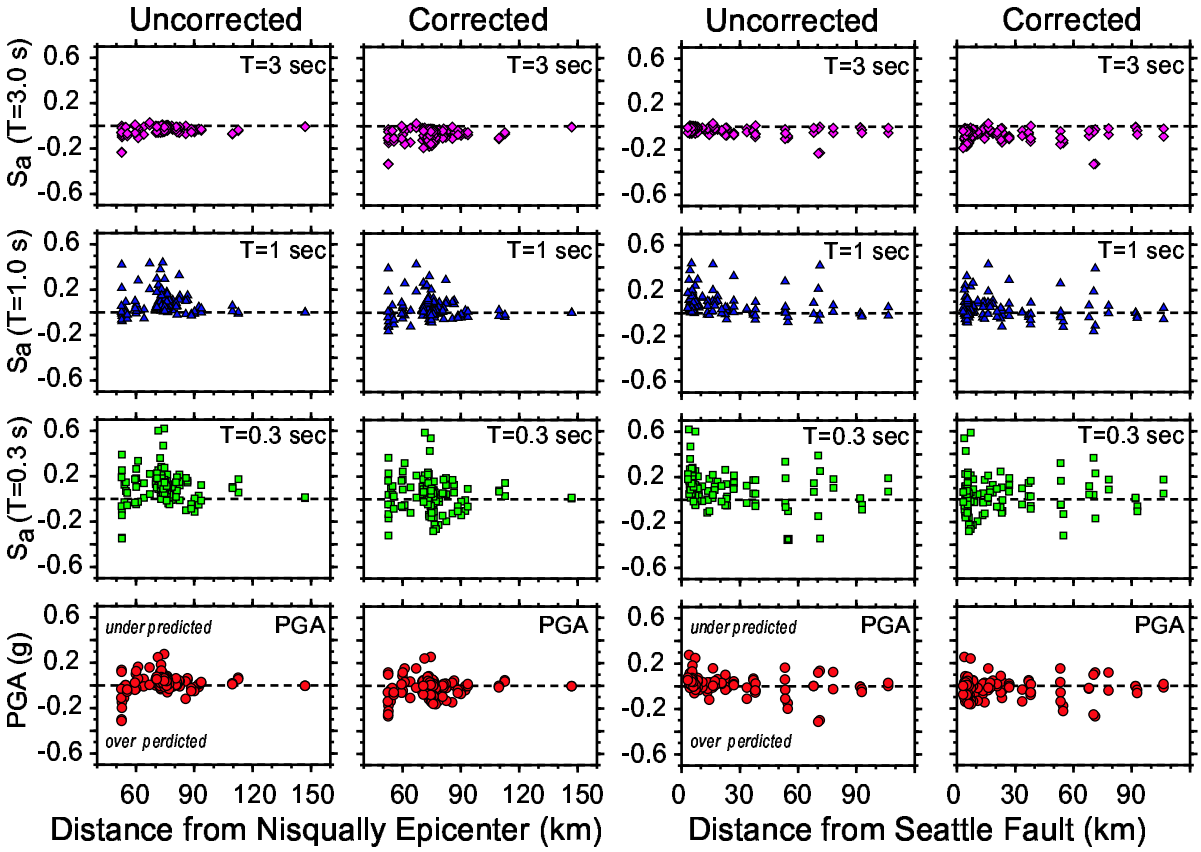

Figure 18. Uncorrected and site and basin depth corrected PGA and S_a residuals between predicted and observed ground motions in units of (g). These ground motions are plotted versus distance from the surface trace of the Seattle fault and Nisqually fault plane.

Table 8. Correlation analysis of ground motion residuals: Correlation coefficients *r*, significance level Ψ

Ground Motion	Distance From	Corrected/Uncorrected	*r*	ψ
PGA	Seattle Fault	Uncorrected	-0.31	0.00047
	Seattle Fault	Corrected	-0.046	0.62
	Epicenter	Uncorrected	0.11	0.20
	Epicenter	Corrected	0.096	0.30
S_a T=1 second	Seattle Fault	Uncorrected	-0.21	0.021
	Seattle Fault	Corrected	-0.12	0.18
	Epicenter	Uncorrected	-0.081	0.38
	Epicenter	Corrected	-0.048	0.60
S_a T=3 seconds	Seattle Fault	Uncorrected	-0.34	0.00011
	Seattle Fault	Corrected	-0.065	0.48
	Epicenter	Uncorrected	0.16	0.081
	Epicenter	Corrected	0.16	0.080

SHAKE-MAP RESULTS

We use a procedure similar to that developed of Wald et al. [1999] to generate shake-maps of PGA and S_a for the 2001 Nisqually (Figure 19) and 1965 Seattle-Tacoma (Figure 20) earthquakes. We use the simulation method rather than GMA models to compute the ground motions for a 2º by 2º area centered over the Puget Sound with a grid spacing of 10×10 km. We generated synthetic acceleration time series to measure PGA values and also compute absolute acceleration spectra with 5% damping to measure S_a at periods of 0.3, 1, and 3 seconds. The peak horizontal ground motions between the two components are averaged before the spatial interpolation step. Spatial interpolation is made using a bicubic scheme [Wessel and Smith, 1991] to a grid spacing of approximately 100×100 meters. The continuous site and basin corrections are digitized using a grid spacing of 100×100 meters and applied to the ground motions.

SHAKE-MAP DISCUSSION

The main feature of the shake-maps is the general decay or attenuation of ground motions away from the epicenter or source region. The ground motions in the near-fault region are also elongated in the strike direction and offset from the epicenter to the southwest. This could be cause by the directivity and finite-fault effects. The depth of the earthquake has a big effect on accelerations where larger accelerations and strong directivity or radiation patterns effects can be observed in the near-field region of shallow crustal earthquakes. The spatial ground motions of deep earthquakes are relatively smoother. The uncorrected shake-maps show symmetric regions or ring patterns of higher ground motions, due to the velocity model and radiation pattern. The other main feature is the basin and site geology effects which cause different amplifications depending on period and ground motion level (Table 4).

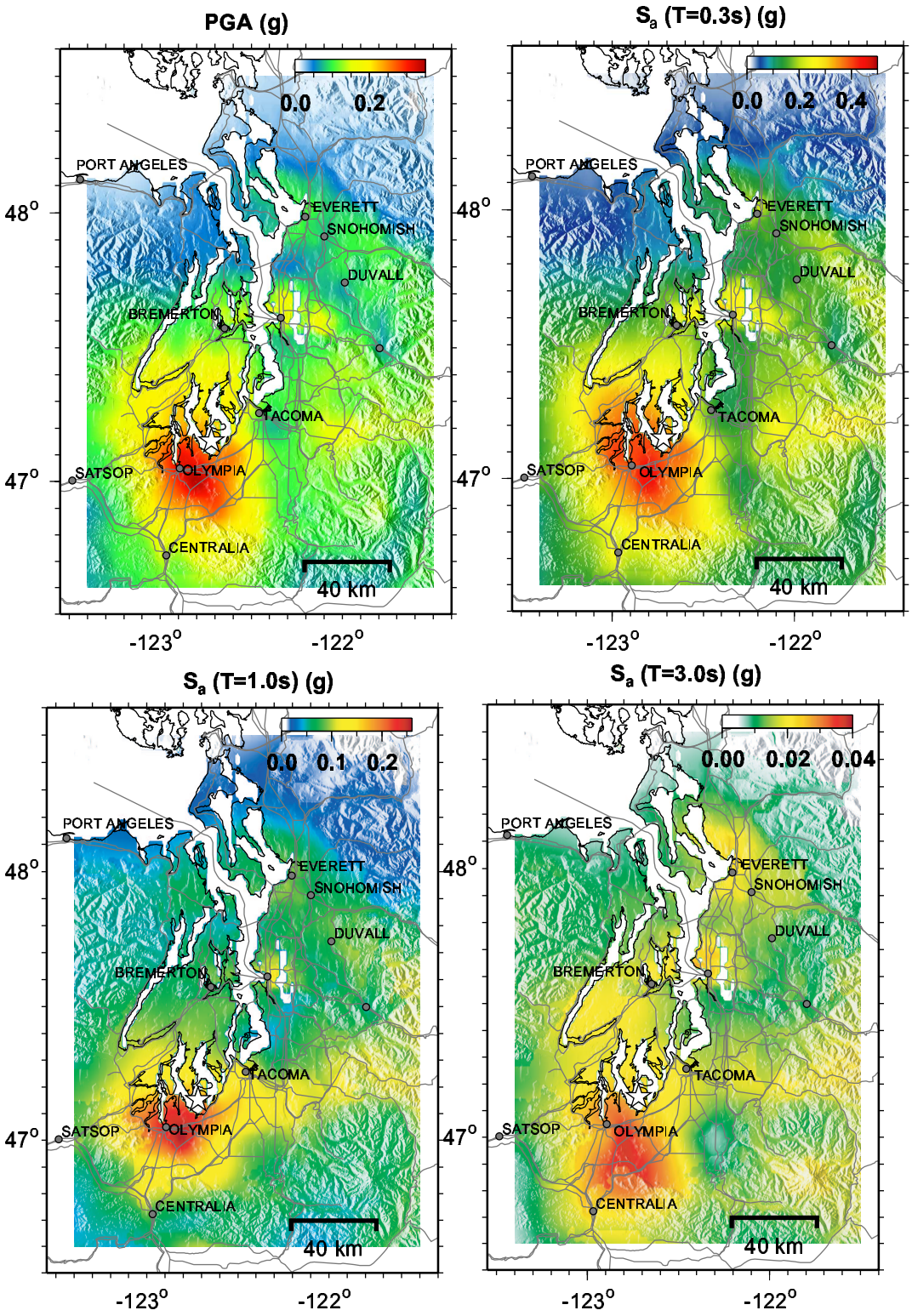

Figure 19. Shake-map of the Puget Sound region for the 2001 Nisqually earthquake. (Top left) Mean horizontal ground accelerations. (Top right) Mean horizontal S_a with 5% damping at period of 0.3 sec. (Bottom left) Mean horizontal S_a with 5% damping at period of 1 sec. (Bottom right) Mean horizontal S_a with 5% damping at period of 3 sec. Notice the scales are different for each panel.

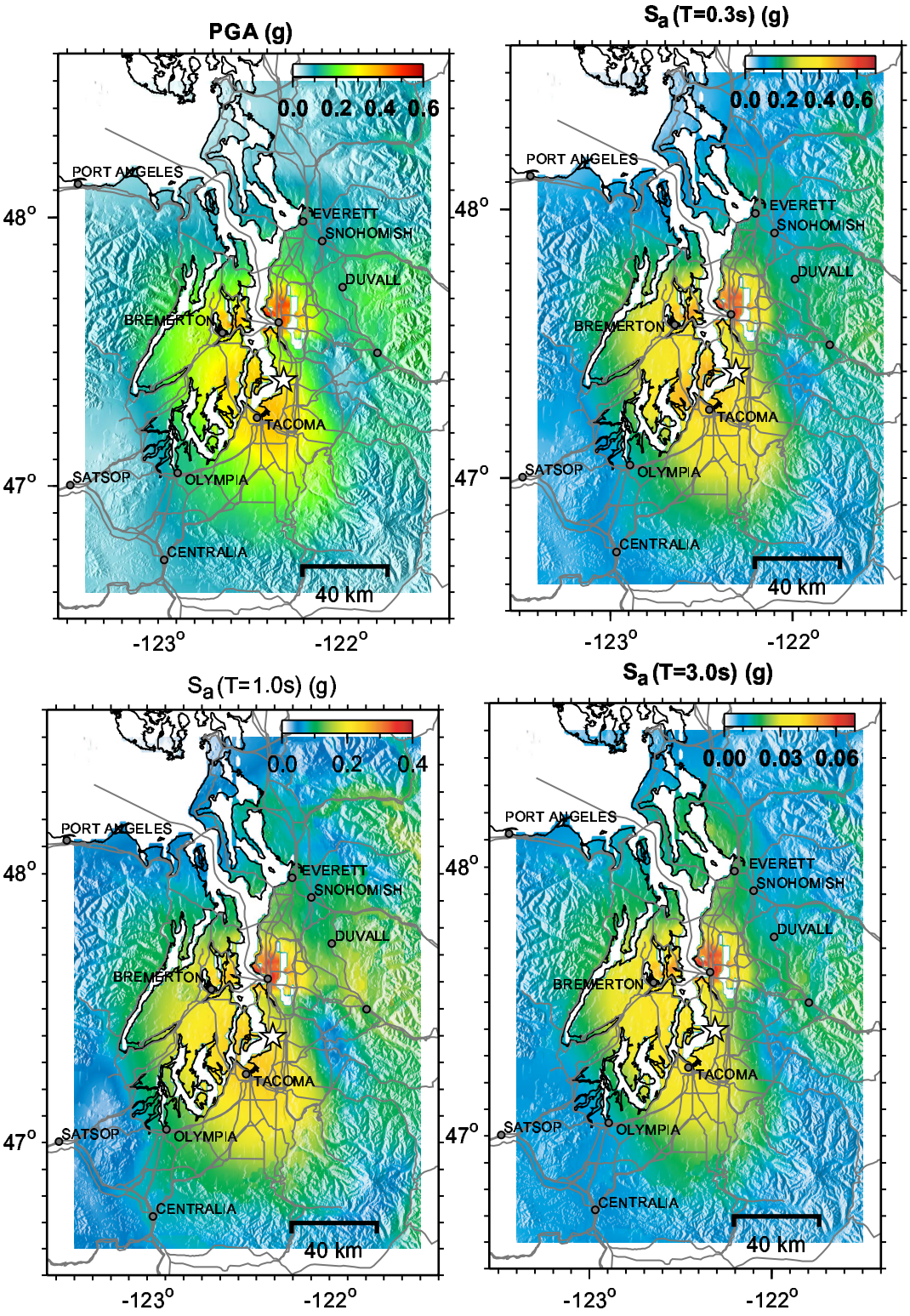

Figure 20. Shake-map of the Puget Sound region for the 1965 Seattle-Tacoma earthquake. (Top left) Mean horizontal ground accelerations. (Top right) Mean horizontal S_a with 5% damping at period of 0.3 sec. (Bottom left) Mean horizontal S_a with 5% damping at period of 1 sec. (Bottom right) Mean horizontal S_a with 5% damping at period of 3 sec. Notice the scales are different for each panel.

The shake-maps for the 2001 Nisqually earthquake (Figure 19) show a similar distribution of ground motions between PGA and S_a at a period of 0.3 seconds. This is expected considering that PGA is a very short period estimate of the ground acceleration. The obvious difference is for S_a at 3 seconds period where the attenuation is much more gradual. The expected regions of light to moderate damage and strong shaking (20-40% g) are localized up-dip from the epicenter and elongated along fault strike. The other areas are in and around the Seattle basin (20% g) where most of the moderate damage was observed. The observed PGA is highly variable and does not correlate very well with the PGA shake-map. Observed S_a at 0.3 and 1.0 sec and damage correlate better than PGA. We expect variability in damage due to variations in age and construction materials used in buildings and transportation systems. Overall, this method generates shake-maps that perform well in predicting observed S_a and observed damage.

The shake-maps generated for the 1965 Seattle-Tacoma earthquake indicates that the distribution of ground motions were very different than those from the 2001 Nisqually earthquake. A repeat of the 1965 earthquake is expected to generate larger ground motions in the Seattle basin than in the near fault region. The expected PGA and S_a at 0.3 seconds is 2 or 3 times higher (up to 60% g) in the Seattle basin than from the 2001 Nisqually earthquake. At this severe level of shaking, one can expect moderate to heavy damage [e.g, Von Hake and Cloud, 1965]. The long period S_a at 3 sec is predicted to be about 6% g in the Seattle basin. Olympia and Everett is expected to experience only moderate PGA levels around 10-20% g while Tacoma can experience peak accelerations of 30% g.

The QTM classification scheme developed by Park and Elrick [1998] and Wills et al. [2000] for California and applied by Wald et al [1999] to shake-maps have a shear-wave velocity of about 590-700 m/s for Mesozoic rock (Table 4). We do not account for this in the Green's functions where the surface velocity is 2.5 km/s in the calibrated model (Table 3). The expected difference in amplification due to the simple impedance contrast between 0.59 km/s and 2.5 km/s is a factor of 2. This was confirmed using f-k synthetics computed between 0 and 200 km by adding a 30 meter thick surface layer with a shear-wave velocity of 590 m/s on top of the calibrated velocity model used to calculate the Green's functions. The resulting difference in amplification for peak ground motion was between 1.6 and 2.2 from the original model. The 30 meter thick low velocity surface layer also generated a strong resonance at 5 Hz with amplification of 8.

The shear-wave velocity for Mesozoic or bedrock in the Puget Sound is probably higher than 590 m/s because the residuals between predicted and observed Sa suggest only an under prediction of about 1.2 and a good fit for PGA. To accommodate for an extra factor of 2 in amplification, we would need to increase the duration of the Kostrov source-time function or increase Q in the shallow layers in order to lower the contribution to the high-frequency spectrum.

Site response studies using spectral ratios suggest amplifications of only 2 between the Duwamish Valley and downtown Seattle, on compacted Quaternary glacial outwash (V_s^{30}=360-385 m/s) consistent with shear-wave velocity of Q class [Hartzell et al, 1999]. The amplifications using the current amplification for Quaternary soils and basin depth effect would account for this amplification factor of 2. Tertiary sandstone is assumed to have shear-wave velocity of 1225 km/s in the Puget Sound [Hartzell et al, 2000] which is much higher than 406 m/s assumed for T class [Park and Elrick, 1998]. Frankel et al [1999] also estimated the site amplification using spectral ratios including those at Tertiary rock sites. They find amplification at or below 1. It is possible that the Tertiary and Mesozoic bedrock for the Puget Sound region has a much higher V_s^{30} than that used in southern California possibly due to compaction and weathering caused by repeated glaciations.

The basin-depth effect was developed for Los Angeles basin in southern California and its application to the Puget Sound was a quick fix in the absence of any other viable options. It is interesting to note that the large depth of the earthquake beneath the basins may cause more of a focusing effect adopted by the Field model than that of a true basin effect where waves from shallow earthquakes are trapped within the basin. This is may be evident in the improvement of the residuals after the use of Field's basin-depth

effect correction and in the insensitivity of longer period S_a at 3 seconds to site and basin effects.

We neglect the effect of soil nonlinearity and liquefication; therefore ground motions may be underestimated or overestimated. Liquefication was observed at several sites in and around urban Seattle where there is the largest concentration of modified land and artificial fill. The expected uncertainties according to the residuals from observed data and predicted values range around 10% g. One limitation of the QTM classification scheme is that the Q class clumps all Quaternary sediments which can have a wide range of shear wave velocities. We need a more detailed classification scheme in future studies. Other limitations include the use of only peak ground motion values which do not include the duration of shaking. The addition of PGV and durations will make the maps more useful.

SUMMARY

The following is a summary of this study:

1. We estimated the regional-wave moment tensors and point source parameters for the 1999 and 2001 Satsop, 2001 Nisqually and 2003 Mount Olympus in-slab earthquakes. We filter the data and Green's functions at long periods (200-20 sec). The source parameters for the Nisqually earthquake are (strike/dip/rake) 351°/68°/-98°, M_o=1.11×10^{26} dyne×cm, and centroid depth of 60 km. The seismic moments and normal faulting focal mechanisms are consistent with previous estimates and the centroid depths (40 km for Satsop and 60 km for Nisqually) indicate that these earthquakes occurred at the inferred top of the subducting Juan de Fuca slab. We validate the moment tensor results by predicting the near-source (<100 km) ground displacements at intermediate periods (T > 1 second).
2. A one-dimensional velocity model is calibrated for ray-paths crossing the Puget Sound using the point source parameters of the 2001 Satsop (M_w 4.7) earthquake recorded at station Longmire (LON Δ=137 km ϕ=109°). The data and synthetics are filtered at intermediate periods appropriate for calibrating Green's functions used in slip model inversions. The new velocity model has larger upper-crustal velocities and smaller mid- to lower-crustal velocities. The low velocity zone in the slab crust is retained from the initial model (PS-9) derived from teleseismic P-waves [Langston and Blum, 1977] and probably poorly resolved in the inversion. This model improves the fit to observed ground motions including the amplitude and phase arrival times for P-waves, S-waves, and S-wave coda.
3. We performed an inversion for the variable slip and rake model from the 1965 Seattle-Tacoma earthquake using 32 teleseismic P- and SH-waves digitized. The teleseismic arrivals from WWSSN stations were manually digitized from microfiche prints. Their instrument responses are convolved onto the Green's functions before the inversion. The finite-fault parameters (strike/dip/rake) 344°/70°/-75° and depth of 60 km are assumed from the study of Langston and Blum [1977]. We assume a fault length of 30 km along strike and down-dip length of 20 km using a grid spacing of 2 by 2 km. We use rise times between 1-3 seconds and a maximum rupture velocity of 3.2 km/s. The rupture is parameterized using 5 time windows at 1 second increments. The slip model consists of two small asperities about 4 and 8 km^2 in area just south and updip from the hypocenter with maximum slips of 2 and 2.8 m. The total seismic moment is 9.43×10^{25} dyne×cm (M_w 6.63).
4. We performed an inversion for variable slip and rake form the 2001 Nisqually earthquake using locally recorded ground velocities filtered between 0.05 and 0.5 Hz from 12 stations, 30 teleseismic P-waves, 7 teleseismic SH-waves, and horizontal co-seismic displacements recorded from 8 GPS receivers. The finite-fault parameters are assumed from the regional-wave moment tensor study. The Green's functions for the local ground motions were computed using the calibrated velocity model while the teleseismic ground motions were computed using the PS-9 velocity model. We assume a fault length of 30 km along strike and down-dip length of 24 km

using a grid spacing of 3 by 3 km. We use rise times between 1-3 sec and a maximum rupture velocity of 3.2 km/s. The rupture was parameterized using 6 time windows at 1 second intervals. The slip model consists of a small 12 km^2 area centered 3 km down dip from the hypocenter with a maximum slip of 3.35 meters. The total seismic moment is 1.59×10^{26} dyne×cm (M_w 6.74). The estimate seismic moment is consistent with geodetic and regional moment tensor inversions.

5. GMA models from Youngs et al [1997] for rock sites, Somerville and Smith [1991], and Crouse [1991] best fit the observed PGA from the 2001 Nisqually earthquake. For distances greater than 100 km the PGA appear to attenuate faster than these GMA models. The GMA models from Youngs et al [1997] for soil sites over predict and Atkinson and Boore [1997] under predict the observed PGA but the majority of the observations are within one standard deviation (e.g., σ=0.78 for Youngs et al [1997], σ=0.77 Crouse [1991]).
6. Observed PGAs were classified based on surface geology using the QTM scheme. GMA models using the functional form of log average relationship indicate that Tertiary sites have a significantly higher attenuation than Quaternary sites.
7. Predicted PGAs, using the simulation procedure with corrections for site and basin-depth, fit the log average relationship of the observed PGA. The fit was also consistent with S_a at periods of 0.3 and 1.0 seconds. There was a large misfit at 3 sec but this can be considered an artifact of the uneven distance distribution in the data. A fit using bins with equal distance weighting is more consistent with the S_a observations at 3 sec.
8. We calculate the residuals between observed and predicted ground motions. The site and basin-depth corrections removed the bias in the residuals but there were no improvement in the spread of the residuals. The S_a at T=3 seconds did not exhibit large residuals before or after the corrections. This suggests that longer period ground motions in the Seattle basin are not affected as much by basin-depth and site effects. One explanation for this is the large depth of the Nisqually earthquake (60 km), directly beneath the basin, resulting in an effect similar to that of a lens which focuses the incident seismic rays. Traditionally a basin effect is thought of as waves which enter the basin from a shallow depth focus and then become trapped within the basin edges.
9. There is a significant correlation 20-30% of the residuals relative to the distance from the trace of the Seattle fault, indicating a 3-D basin edge effect. The site and basin-depth corrections removed this correlation suggesting that the basin-depth corrections of Field [2000] are somewhat applicable in the Puget Sound region.
10. Shake-maps of the 2001 Nisqually earthquake show a similar distribution of ground motions between PGA and S_a (all S_a are have 5% damping) at a period of 0.3 seconds. The main difference is from S_a at 3 seconds period, where the attenuation is more gradual. The expected regions of light to moderate damage and strong shaking (20-40% g) are localized up-dip from the epicenter and elongated along fault strike. The other area is in and around the Seattle basin (20% g) where most of the moderate damage was observed. The observed PGA is highly variable and do not correlate very well with the PGA shake-map. Observed S_a at 0.3 and 1.0 sec and damage do correlate better than PGA.
11. The shake-maps for the 1965 Seattle-Tacoma earthquake indicate that PGA and S_a, at a period of T=0.3 seconds are 2 or 3 times higher (up to 60% g) in the Seattle basin than from the 2001 Nisqually earthquake. These are about twice as high as those around the epicenter near Tacoma. At this severe level of shaking, one can expect moderate to heavy damage. The long period S_a at T=3 seconds are predicted to be only about 6% g in the Seattle basin. Olympia and Everett is expected to experience only moderate levels of PGA around 10-20% g while Tacoma can experience accelerations of 30% g.

REFERENCES

Atkinson, G. M., Attenuation and source parameters of earthquakes in the Cascadia region, Bull. Seismol. Soc. Am., 85, 1327-1342, 1995.

Atkinson, G. M., and D. M. Boore, Stochastic point-source modeling of ground motions in the Cascadia region, Seismol. Res. Lett., 68, 74-85, 1997.

Atkinson, G. M., and D. M. Boore, Empirical ground-motion relations for subduction zone earthquakes and their application to Cascadia and other regions, submitted to Bull. Seismol. Soc. Am., 2003.

Baker, G. E., and C. A. Langston, Source parameters of the 1949 magnitude 7.1 south Puget Sound, Washington, earthquake as determined from long-period body waves and strong motions, Bull. Seismol. Soc. Am., 77, 1530-1557, 1987.

Barksdale, J. D., and H. A. Coombs, The Puget Sound earthquake of Feb. 14, Bull. Seismol. Soc. Am., 36, 349-354, 1946.

Berteussen, K., Moho depths determinations based on spectral-ratio analysis of NOSAR long-period P-waves, Phys, Earth., Planet. Inter., 15, 1530-1557, 1987.

Brocher, T. M., T. Parsons, R. J. Blakely, N. I. Christensen, M. A. Fisher, R. E. Wells, and the SHIPS Working Group, Upper crustal structure in Puget Lowland, Washington: Results from the 1998 Seismic Hazards Investigation in Puget Sound, J. Geophys. Res., 106, 13,541-13,564, 2001.

Burdick, L. J., and C. A. Langston, Modeling crustal structure through the use of converted phases in teleseismic body-wave forms, Bull. Seismol. Soc. Am., 67, 677-691, 1977.

Carver, D., A. D. Frankel, W. T. Bice, B. Norris, and N. Dickman, Configuration of the Seattle Urban Seismic Array for the February 28, 2001, M 6.8, Nisqually earthquake and its aftershocks, U. S. Geological Survey, Open File Rpt. 01-344, 2001.

Claerbout, J. F., Earth Sounding Analysis Processing Versus Inversion, Blackwell Scientific Publications, Boston, MA, 1992.

Crouse, C. B., Ground-motion attenuation equations for earthquakes on the Cascadia subduction zone, Earthquake Spectra, 7, 201-236, 1991.

Dobson, D. P., P. G. Meredith, S. A. Boon, Simulation of subduction zone seismicity by dehydration of serpentine, Science, 298, 1407-1410, 2002.

Dreger, D., and A. Kaverina, Seismic remote sensing for the earthquake source process and near-source strong shaking: A case study of the October 16, 1999 Hector Mine Earthquake, Geophys. Res. Lett., 27, 1941-1933, 2000.

Field, E. H., A modified ground-motion attenuation relationship for southern California that accounts for detailed site classification and a basin-depth effect, Bull. Seismol. Soc. Am., 90, S209-S221, 2000.

Field, E. H., Earthquake ground-motion amplification in southern California, U. S. Geological Survey, Open File Rpt. 01-164, 2001.

Frankel, A., D. Carver, E. Cranswick, M. Meremonte, T. Bice, and D. Overturf, Site response for Seattle and source parameters of earthquakes in the Puget Sound region, Bull. Seismol. Soc. Am., 89, 468-483, 1999.

Graves, R. W., A. Pitarka, and P. G. Somerville, Ground motion amplification in the Santa Monica area: Effects of shallow basin-edge structure, Bull. Seismol. Soc. Am., 88, 1224-1242, 1998.

Guatteri, M, P. M. Mai, G. C. Beroza, and J. Boatwright, Strong ground motion prediction from stochastic-dynamic source models, Bull. Seismol. Soc. Am., 93, 301-313, 2003.

Hacker, B. R., G. A. Abers, and S. M. Peacock, Theoretical mineralogy, density seismic wave speeds, and H2O content of the Cascadia subduction zone, with implications for intermediate-depth seismicity and earthquake hazard, in Intraslab Earthquakes in the Cascadia Subduction System: Science and Hazard, U.S. Geological Survey Circular, in press., 2003.

Hartzell, S. H., and T. H. Heaton, Inversion of strong motion and teleseismic waveform data for the fault rupture history of the 1979 Imperial Valley, California earthquake, Bull. Seismol. Soc. Am., 73, 1553-1583, 1983.

Hartzell, S., D. Carver, E. Cranswick, and A. Frankel, Variability of site response in Seattle, Washington, Bull. Seismol. Soc. Am., 90, 1237-1250, 2000.

Heaton, T. H., Evidence for and implications of self-healing pulses of slip in earthquake rupture, Phys. Earth and Planet. Int., 64, 1-20, 1990.

Ichinose, G. A., Thio, Hong Kie, and P. G. Somerville, Source characteristics of modern and historical in-slab Cascadia earthquakes applicable to strong ground motion prediction, U. S. Geological Survey, NEHRP Annual Project Summary Award #02HQGR0018, 2002a.

Ichinose, G. A., and Thio, Hong Kie, Source parameters of In-slab Cascadia subduction zone earthquakes (abstract), Seismol. Res. Lett. 73, 214, 2002b.

Ichinose, G. A., J. G. Anderson, K. D. Smith, and Y. Zeng, Source parameters of eastern California and western Nevada earthquakes from regional moment tensor inversion, Bull. Seismol. Soc. Am., 93, 61-84, 2003.

Ihnen, S. M. and D. M. Hadley, Prediction of strong ground motion in the Puget Sound region: the 1965 Seattle earthquake, Bull. Seismol. Soc. Am., 76, 905-922, 1986.

Jost, M. L., and R. B. Herrmann, A students guide to and review of moment tensors, Seismol. Res. Lett., 60, 37-57, 1989.

Kirby, S., E. R. Engdahl, and R. Denlinger, Intermediate depth, intraslab earthquakes and arc volcanism as physical expressions of crustal and uppermost mantle metamorphism in subducting slabs, in Subduction from top to bottom, (editor) Bebout, G. D., Scholl, D., Kirby, S., and Platt, J., American Geophysical Union, Geophys. Mono. No. 96, 195-214, 1996.

Langston, C. A., Corvallis, Oregon, crustal and upper mantle receiver structure from teleseismic P and S waves, Bull. Seismol. Soc. Am., 67, 713-724, 1977.

Langston, C. A., Evidence for the subducting lithosphere under southern Vancouver Island and western Oregon from teleseismic P-wave conversions, J. Geophys. Res., 86, 3857-3866, 1981.

Langston, C. A., and D. E. Blum, The April 29, 1965, Puget Sound earthquake and the crustal and upper mantle structure of western Washington, Bull. Seismol. Soc. Am., 67, 693-711, 1977.

Lawson, C. L., and R. J. Hansen, Solving Least Squares Problems, Englewood Cliffs, New Jersey, Prentice-Hall, 1974.

Miyake, H., T. Iwata, Sekiguchi, H., and K. Irikura, Appropriate slip velocity time function of on-/off- asperity for broadband ground motion simulation, Eos. Trans. AGU, 82(47), Fall Meet. Suppl., F906, 2001.

Mueller, G., The reflectivity method: a tutorial, J. Geophys., 58, 153-174, 1985.

Nisqually Earthquake Clearinghouse Group, The Nisqually, Washington, Earthquake February 28, 2001, EERI Learning from Earthquakes Preliminary Reconnaissance Report, Earthquake Engineering Research Institute 2001-01, Oakland, CA, 2001.

Nuttli, O. W., The western Washington earthquake of April 13, 1949, Bull. Seismol. Soc. Am., 42, 21-28, 1950.

Okada, Y., Internal deformation due to shear and tensile faults in a half-space, Bull. Seismol. Soc. Am., 82, 1018-1040, 1992.

Owens, T. J., R. S. Crosson, and M. A. Hendrickson, Constraints on the subduction geometry beneath western Washington from broadband teleseismic waveform modeling, Bull. Seismol. Soc. Am., 78, 1319-1334, 1988.

Park, S., and S. Elrick, Predictions of shear-wave velocities in southern California using surface geology, Bull. Seismol. Soc. Am., 88, 677-685, 1998.

Peacock, S. M., and K. Wang, Seismic consequences of warm versus cool subduction metamorphism: Examples from southwest and northwest Japan, Science, 286, 937-939, 1999.

Ritsema, J., and T. Lay, Long period regional wave moment tensor inversion for earthquakes in the western United States, J. Geophys. Res., 100, 9853-9864, 1995.

Schuster, E. J., Geologic Map of Washington, Washington State Dept. Natural Resources, Division of Geology and Earth Resources, Olympia, WA, 2002.

Somerville, P. G., K. Irikura, R. Graves, S. Sawada, D. Wald, N. Abrahamson, Y. Iwasaki, T. Kagawa, N. Smith, and A. Kowada, Characterizing crustal earthquake slip models for the prediction of strong ground motion, Seismol. Res. Lett., 70, 59-80, 1999.

Somerville, P. G., and N. F. Smith, Simulation and empirical studies of strong ground motion attenuation in the Seattle-Portland regions, U. S. Geological Survey, Final Technical Report, Award #14-08-0001-G1516, 1991.

Symons, N. P., and R. S. Crosson, Seismic velocity structure of the Puget Sound region from 3-D non-linear tomography, Geophys. Res. Lett., 24, 2593-2596, 1997.

Von Hake, C. A., and W. K. Cloud, The Puget Sound Earthquake of April 29, 1965, U. S. Department of Commerce, Environmental Science Services Administration, Coast and Geodetic Survey, U. S. Government Printing Office, pp 32-51, 1965.

Wald, D. J., and T. H. Heaton, Spatial and temporal distribution of slip for the 1992 Landers, California earthquake, Bull. Seismol. Soc. Am., 84, 668-691, 1994.

Wald, D. J., V. Quitoriano, T. H. Heaton, H. Kanamori, C. W. Scrivner, and C. B. Worden, TriNet "Shake Maps": Rapid generation of peak ground motion and intensity maps for earthquakes in southern California, Earthquake Spectra, 15, 537-556, 1999.

Weaver, C. S., and G. E. Baker, Geometry of the Juan de Fuca plate beneath Washington and northern Oregon from seismicity, Bull. Seismol. Soc. Am., 78, 264-275, 1988.

Wessel, P., and W. H. F. Smith, Generic Mapping Tools: Free software helps map and display data, Eos, Trans. AGU, 72, 441, 1991.

Wills, C. J., M. Petersen, W. A. Bryant, M. Reichle, G. J. Saucedo, S. Tan, G. Taylor, and J. Treiman, A site-condition map for California based on geology and shear-wave velocity, Bull. Seismol. Soc. Am., 90, S187-S208, 2000.

Xu, Y., and D. A. Wiens, Upper mantle structure of the southwest Pacific from regional waveform inversion, J. Geophys. Res., 102, 27,439-27,451, 1997.

Youngs, R. R., S. J. Chiou, W. J. Silva, J. R. Humphrey, Strong ground motion attenuation relationships for subduction zone earthquakes, 68, 58-73, 1997.

Zeng, Y., and J. G. Anderson, A method for direct computation of the differential seismogram with respect to the velocity change in a layered elastic solid, Bull. Seismol. Soc. Am., 85, 300-307.

APPENDIX A-1

Stations are in alphabetical order from bottom left to top right.

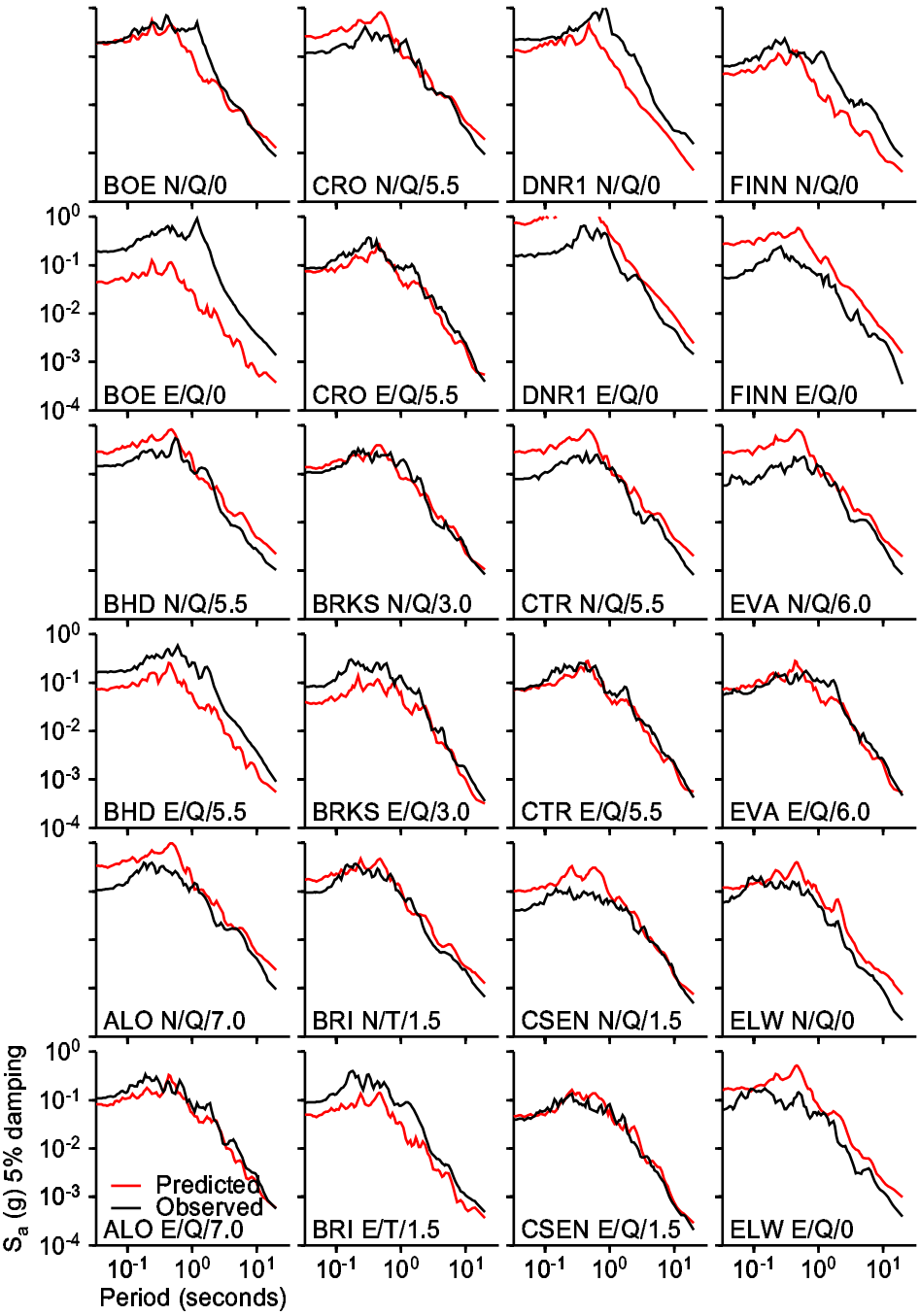

Appendix A-1. Absolute acceleration (Sa) spectra versus period for the north-south (N) and east-west (E) components. The station, component, surface geology, and basin depth beneath the site are labeled for each observed and predicted spectra.

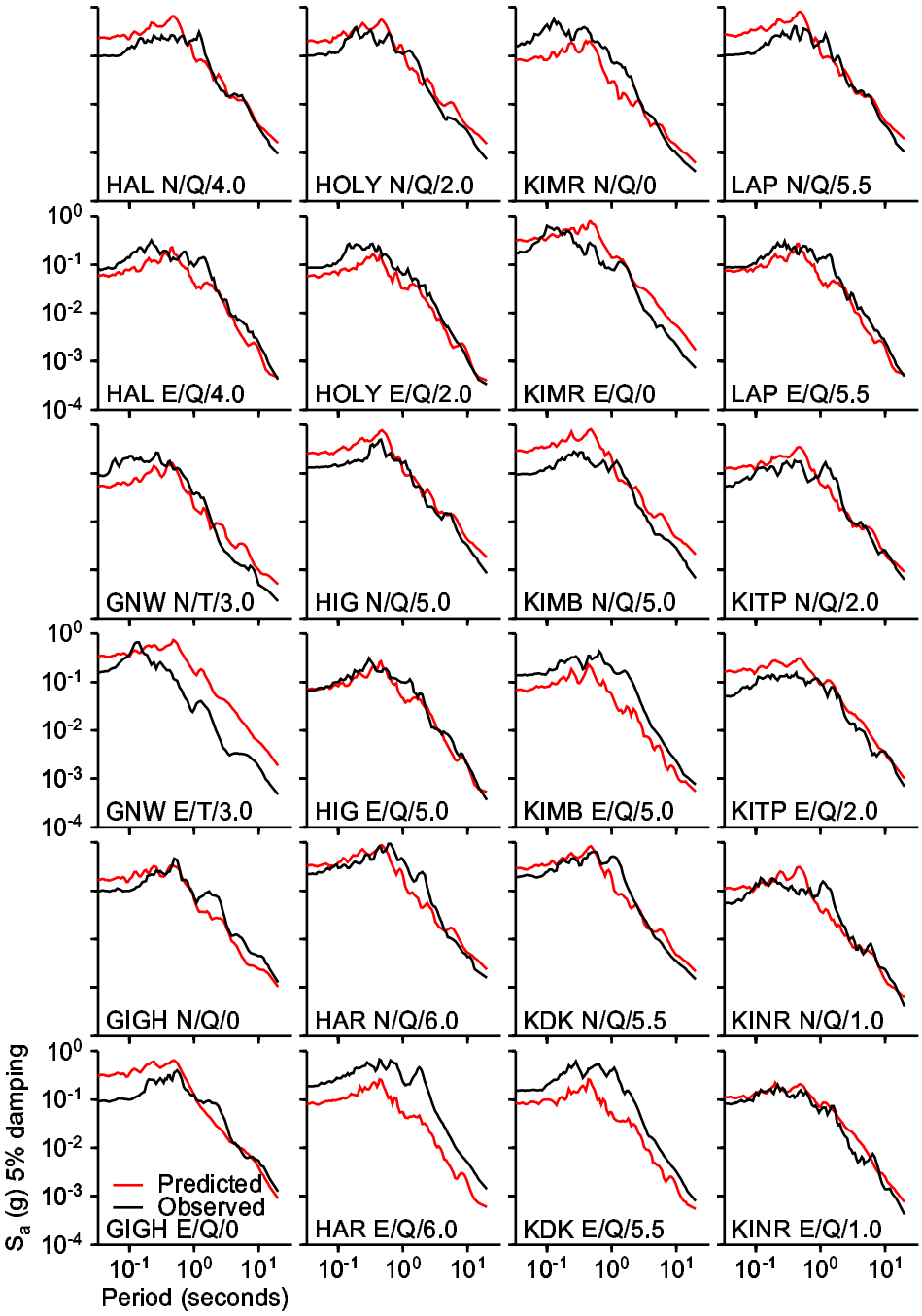

Appendix A-1. Absolute acceleration (Sa) spectra versus period for the north-south (N) and east-west (E) components. The station, component, surface geology, and basin depth beneath the site are labeled for each observed and predicted spectra.

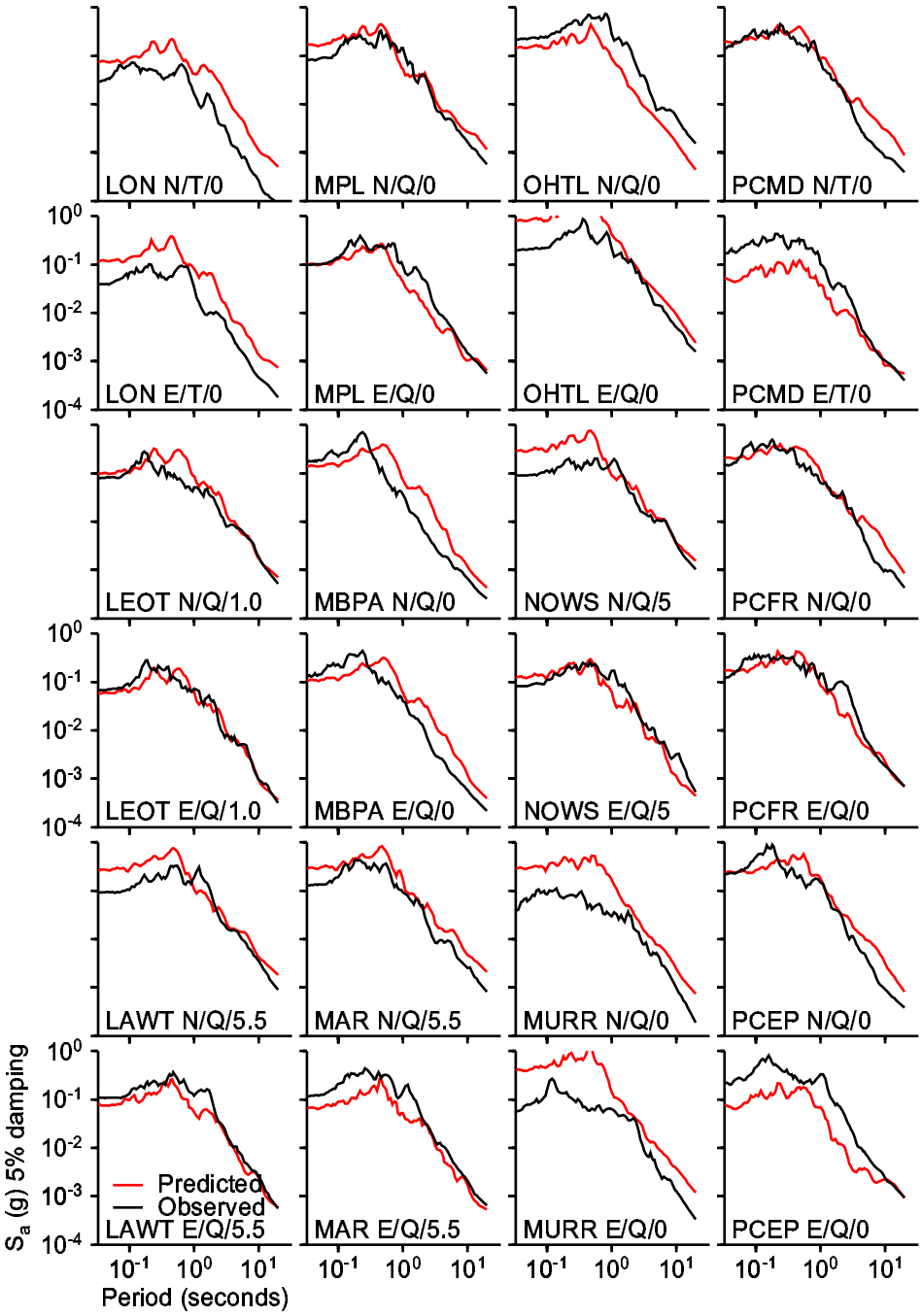

Appendix A-1. Absolute acceleration (Sa) spectra versus period for the north-south (N) and east-west (E) components. The station, component, surface geology, and basin depth beneath the site are labeled for each observed and predicted spectra.

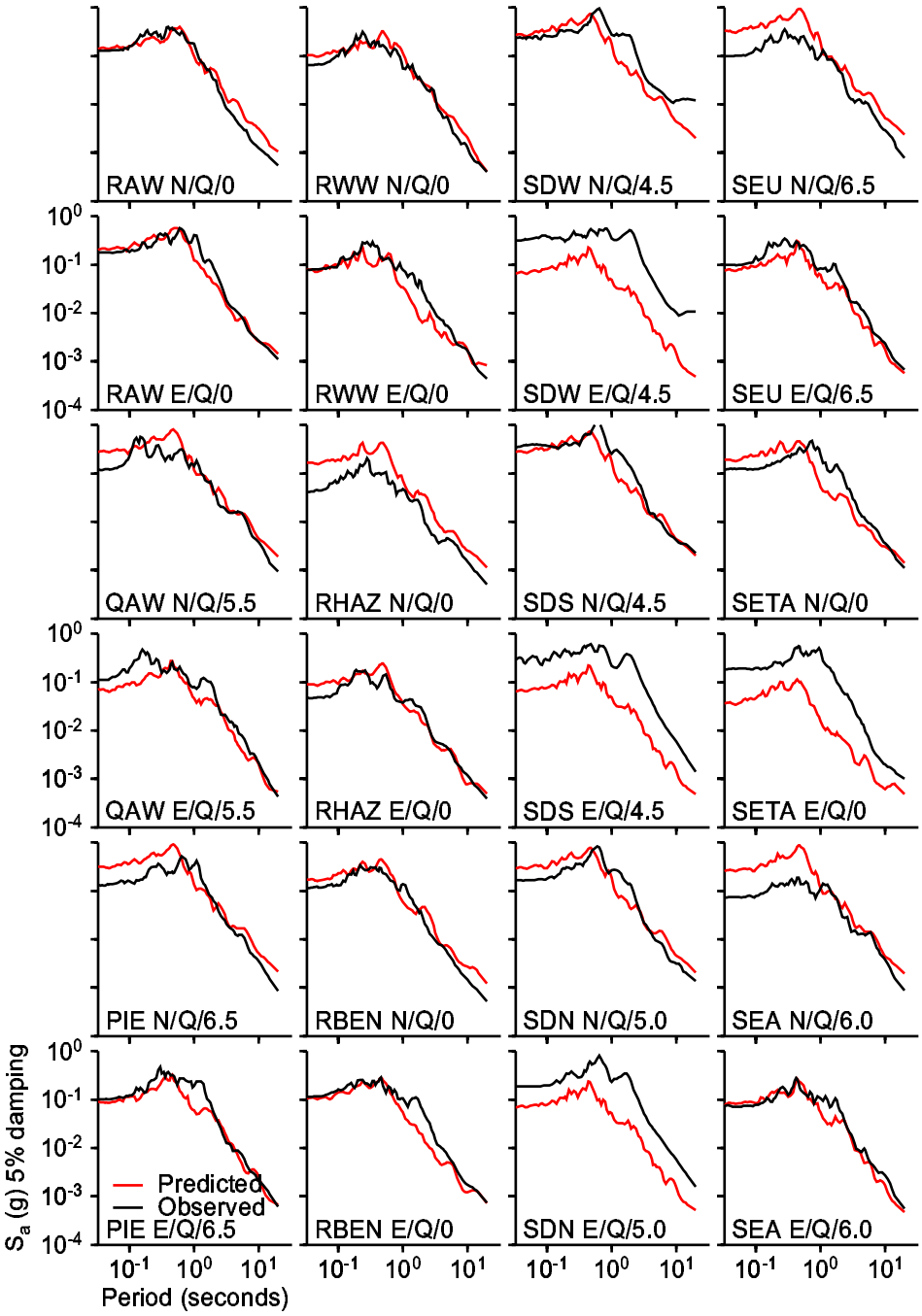

Appendix A-1. Absolute acceleration (Sa) spectra versus period for the north-south (N) and east-west (E) components. The station, component, surface geology, and basin depth beneath the site are labeled for each observed and predicted spectra.

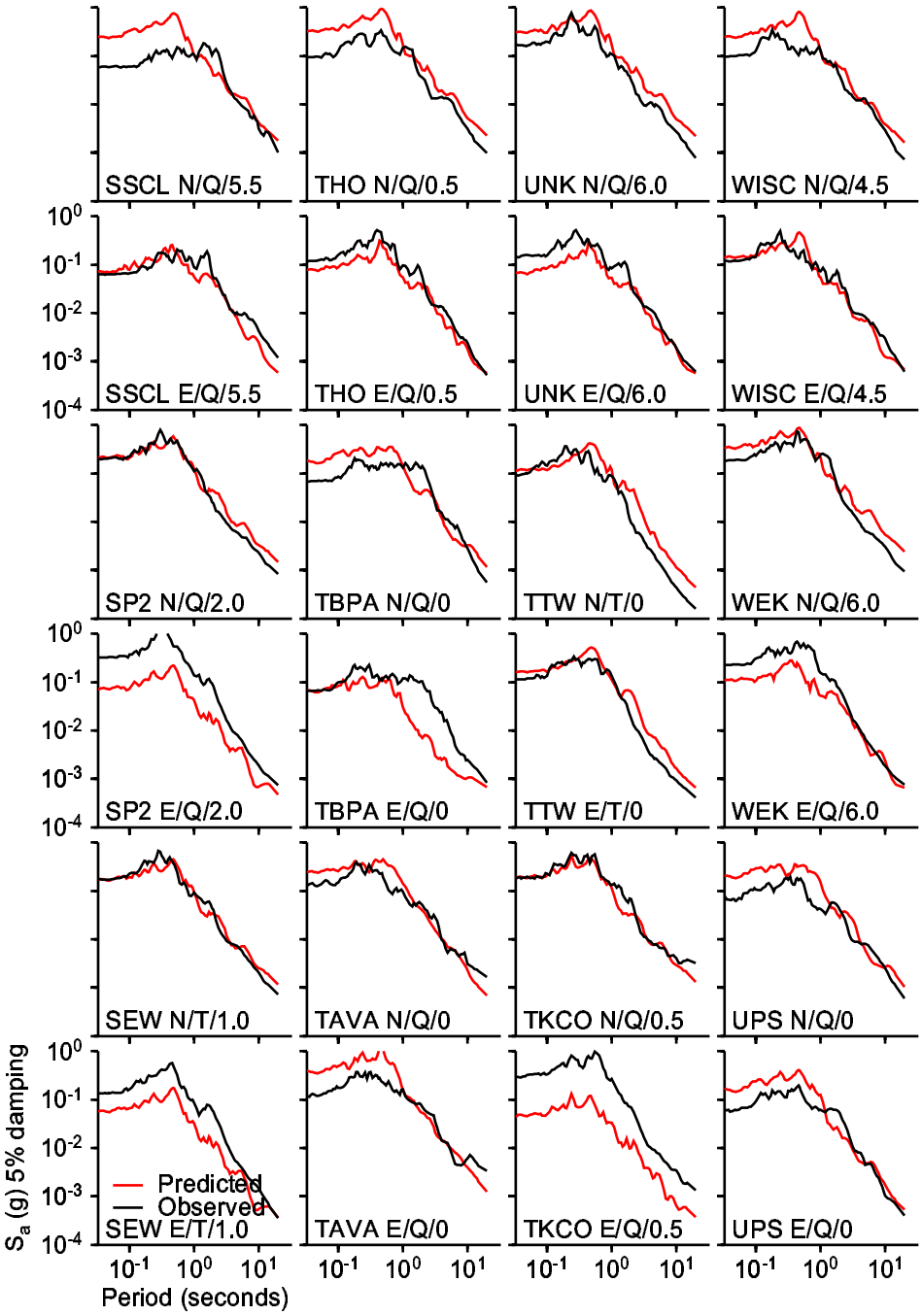

Appendix A-1. Absolute acceleration (Sa) spectra versus period for the north-south (N) and east-west (E) components. The station, component, surface geology, and basin depth beneath the site are labeled for each observed and predicted spectra.